

BLOOMING IN A NONLOCAL, COUPLED PHYTOPLANKTON-NUTRIENT MODEL*

A. ZAGARIS[†], A. DOELMAN[†], N. N. PHAM THI[‡], AND B. P. SOMMEIJER[§]

Abstract. Recently, it has been discovered that the dynamics of phytoplankton concentrations in an ocean exhibit a rich variety of patterns, ranging from trivial states to oscillating and even chaotic behavior [J. Huisman, N. N. Pham Thi, D. M. Karl, and B. P. Sommeijer, *Nature*, 439 (2006), pp. 322–325]. This paper is a first step towards understanding the bifurcational structure associated with nonlocal coupled phytoplankton-nutrient models as studied in that paper. Its main subject is the linear stability analysis that governs the occurrence of the first nontrivial stationary patterns, the *deep chlorophyll maxima* (DCMs) and the *benthic layers* (BLs). Since the model can be scaled into a system with a natural singularly perturbed nature, and since the associated eigenvalue problem decouples into a problem of Sturm–Liouville type, it is possible to obtain explicit (and rigorous) bounds on, and accurate approximations of, the eigenvalues. The analysis yields bifurcation-manifolds in parameter space, of which the existence, position, and nature are confirmed by numerical simulations. Moreover, it follows from the simulations and the results on the eigenvalue problem that the asymptotic linear analysis may also serve as a foundation for the secondary bifurcations, such as the oscillating DCMs, exhibited by the model.

Key words. phytoplankton, singular perturbations, eigenvalue analysis, Sturm–Liouville, Airy functions, WKB

AMS subject classifications. 35B20, 35B32, 34B24, 34E20, 86A05, 92D40

DOI. 10.1137/070693692

1. Introduction. Phytoplankton forms the foundation of most aquatic ecosystems [16]. Since it transports significant amounts of atmospheric carbon dioxide into the deep oceans, it may play a crucial role in climate dynamics [6]. Therefore, the dynamics of phytoplankton concentrations have been studied intensely and from various points of view (see, for instance, [7, 11, 15] and the references therein). Especially relevant and interesting patterns exhibited by phytoplankton are the *deep chlorophyll maxima* (DCMs), or *phytoplankton blooms*, in which the phytoplankton concentration exhibits a maximum at a certain, well-defined depth of the ocean (or, in general, of a vertical water column). Simple, one-dimensional, scalar—but nonlocal—models for the influence of a depth-dependent light intensity on phytoplankton blooms have been studied since the early 1980s [14]. The nonlocality of these models is a consequence of the influence of the accumulated plankton concentration on the light intensity at a certain depth z (see (1.2) below). Numerical simulations and various mathematical approaches (see [5, 7, 8, 10, 12]) show that these models may, indeed, exhibit DCMs, depending on the manner in which the decay of the light intensity with depth is modeled and for certain parameter combinations.

*Received by the editors June 5, 2007; accepted for publication (in revised form) October 6, 2008; published electronically January 30, 2009. This work was supported by the Netherlands Organisation for Scientific Research (NWO).

<http://www.siam.org/journals/siap/69-4/69369.html>

[†]Korteweg-de Vries Institute, University of Amsterdam, Plantage Muidergracht 24, 1018 TV Amsterdam, The Netherlands, and Centrum Wiskunde & Informatica (CWI), P.O. Box 94079, 1090 GB Amsterdam, The Netherlands (A.Zagaris@cw.nl, A.Doelman@cw.nl).

[‡]ABN AMRO Bank N.V., P.O. Box 283, 1000 EA, Amsterdam, The Netherlands (Nga.Pham.Thi@nl.abnamro.com).

[§]CWI, P.O. Box 94079, 1090 GB Amsterdam, The Netherlands (B.P.Sommeijer@cw.nl).

The analysis in [14] establishes that, for a certain (large) class of light intensity functions, the scalar model has a stationary global attractor. This attractor may be trivial; i.e., the phytoplankton concentration W may decrease with time to $W \equiv 0$. If this trivial pattern is spectrally unstable, either the global attractor is a DCM or the phytoplankton concentration is maximal at the surface of the ocean (this latter case is called a *surface layer* (SL) [10, 15]). It should be noted here that *benthic layers* (BLs) [15]—i.e., phytoplankton blooms that become maximum at the bottom of the water column—cannot occur in the setting of [14], due to the choice of boundary conditions. Although the analysis in [14] cannot be applied directly to all scalar models in the literature, the main conclusion—that such models may only exhibit stationary nontrivial patterns (DCMs, SLs, or BLs)—seems to be true for each one of these models.

In sharp contrast to this, it has been numerically discovered recently [11] that systems—i.e., nonscalar models in which the phytoplankton concentration W is coupled to an evolution equation for a nutrient N —may exhibit complex behavior ranging from periodically oscillating DCMs to chaotic dynamics. These nonstationary DCMs have also been observed in the Pacific Ocean [11].

In this paper, we take a first step towards understanding the rich dynamics of the phytoplankton-nutrient models considered in [11]. Following [11], we consider the one-dimensional (i.e., depth-dependent only), nonlocal model,

$$(1.1) \quad \begin{cases} W_t = D W_{zz} - V W_z + [\mu P(L, N) - l] W, \\ N_t = D N_{zz} - \alpha \mu P(L, N) W, \end{cases}$$

for $(z, t) \in [0, z_B] \times \mathbf{R}_+$ and where $z_B > 0$ determines the depth of the water column. The system is assumed to be in the turbulent mixing regime (see, for instance, [5, 10]), and thus the diffusion coefficient D is taken to be identically the same for W and N . The parameters V , l , α , and μ measure, respectively, the sinking speed of phytoplankton, the species-specific loss rate, the conversion factor, and the maximum specific production rate, and they are all assumed to be positive (see Remark 1.1 also). The light intensity L is modeled by

$$(1.2) \quad L(z, t) = L_I e^{-K_{bg}z - R \int_0^z W(\zeta, t) d\zeta},$$

where L_I is the intensity of the incident light at the water surface, K_{bg} is the light absorption coefficient due to nonplankton components, and R is the light absorption coefficient due to the plankton. Note that L is responsible for the introduction of nonlocality into the system. The function $P(L, N)$, which is responsible for the coupling, models the influence of light and nutrient on the phytoplankton growth, and it is taken to be

$$(1.3) \quad P(L, N) = \frac{LN}{(L + L_H)(N + N_H)},$$

where L_H and N_H are the half-saturation constants of light and nutrient, respectively. We note that, from a qualitative standpoint, the particular form of P is of little importance. Different choices for P yield the same qualitative results, as long as they share certain common characteristics with the function given in (1.3); see Remark 1.1. Finally, we equip the system with the boundary conditions

$$(1.4) \quad D W_z - V W|_{z=0, z_B} = 0, \quad N_z|_{z=0} = 0, \quad \text{and} \quad N|_{z=z_B} = N_B,$$

i.e., no-flux through the boundaries except at the bottom of the column where N is at its maximum (prescribed by N_B). We refer the reader to Remark 1.1 for a discussion of more general models. To recast the model in nondimensional variables, we rescale time and space by setting

$$x = z/z_B \in (0, 1) \quad \text{and} \quad \tau = \mu t \geq 0;$$

we introduce the scaled phytoplankton concentration ω , nutrient concentration η , and light intensity j ,

$$\omega(x, \tau) = \frac{l\alpha z_B^2}{DN_B} W(z, t), \quad \eta(x, \tau) = \frac{N(z, t)}{N_B}, \quad j(x, \tau) = \frac{L(z, t)}{L_I};$$

and thus we recast (1.1) in the form

$$(1.5) \quad \begin{cases} \omega_\tau = \varepsilon \omega_{xx} - \sqrt{\varepsilon} a \omega_x + (p(j, \eta) - \ell) \omega, \\ \eta_\tau = \varepsilon \left(\eta_{xx} - \frac{1}{\ell} p(j, \eta) \omega \right). \end{cases}$$

Here,

$$(1.6) \quad j(x, \tau) = \exp \left(-\kappa x - r \int_0^x \omega(s, \tau) ds \right), \quad \text{with} \quad \kappa = K_{bg} z_B \quad \text{and} \quad r = \frac{RD N_B}{l\alpha z_B},$$

and

$$(1.7) \quad \varepsilon = \frac{D}{\mu z_B^2}, \quad a = \frac{V}{\sqrt{\mu D}}, \quad \ell = \frac{l}{\mu}, \quad \text{and} \quad p(j, \eta) = \frac{j\eta}{(j + j_H)(\eta + \eta_H)},$$

where $j_H = L_H/L_I$, $\eta_H = N_H/N_B$. The rescaled boundary conditions are given by

$$(1.8) \quad (\sqrt{\varepsilon} \omega_x - a \omega)(0) = (\sqrt{\varepsilon} \omega_x - a \omega)(1) = 0, \quad \eta_x(0) = 0, \quad \text{and} \quad \eta(1) = 1.$$

These scalings are suggested by realistic parameter values in the original model (1.1) as reported in [11]. Typically,

$$D \approx 0.1 \text{ cm}^2/\text{s}, \quad V \approx 4.2 \text{ cm/h}, \quad z_B \approx 3 \cdot 10^4 \text{ cm}, \quad l \approx 0.01/\text{h}, \quad \text{and} \quad \mu \approx 0.04/\text{h},$$

so that

$$(1.9) \quad \varepsilon \approx 10^{-5}, \quad a \approx 1, \quad \text{and} \quad \ell \approx 0.25$$

in (1.5). Thus, realistic choices of the parameters in (1.1) induce a *natural singularly perturbed structure* in the model, as is made explicit by the scaling of (1.1) into (1.5). In this article, ε will be considered as an asymptotically small parameter, i.e., $0 < \varepsilon \ll 1$.

The simulations in [11] indicate that the DCMs bifurcate from the trivial stationary pattern,

$$(1.10) \quad \bar{\omega}(x, \tau) \equiv 0, \quad \bar{\eta}(x, \tau) \equiv 1 \quad \text{for all } (x, \tau) \in [0, 1] \times \mathbf{R}_+;$$

see also section 3. To analyze this (first) bifurcation, we set

$$(\omega(x, \tau), \eta(x, \tau)) = (\tilde{\omega} e^{\lambda \tau}, 1 + \tilde{\eta} e^{\lambda \tau}), \quad \text{with} \quad \lambda \in \mathbf{C},$$

and consider the (spectral) stability of $(\bar{\omega}, \bar{\eta})$. This yields the linear eigenvalue problem

$$(1.11) \quad \begin{cases} \varepsilon \omega_{xx} - \sqrt{\varepsilon} a \omega_x + (f(x) - \ell) \omega = \lambda \omega, \\ \varepsilon (\eta_{xx} - \frac{1}{\ell} f(x) \omega) = \lambda \eta, \end{cases}$$

where we have dropped the tildes with a slight abuse of notation. The boundary conditions are

$$(1.12) \quad (\sqrt{\varepsilon} \omega_x - a \omega)(0) = (\sqrt{\varepsilon} \omega_x - a \omega)(1) = 0 \quad \text{and} \quad \eta_x(0) = \eta(1) = 0,$$

while the function f is the linearization of the function $p(j, \eta)$,

$$(1.13) \quad f(x) = \frac{1}{(1 + \eta_H)(1 + j_H e^{\kappa x})}.$$

The linearized system (1.11) is *partially decoupled*, so that the stability of $(\bar{\omega}, \bar{\eta})$ as solution of the *two-component system* (1.5) is determined by two *one-component* Sturm–Liouville problems,

$$(1.14) \quad \begin{aligned} \varepsilon \omega_{xx} - \sqrt{\varepsilon} a \omega_x + (f(x) - \ell) \omega &= \lambda \omega, \\ (\sqrt{\varepsilon} \omega_x - a \omega)(0) &= (\sqrt{\varepsilon} \omega_x - a \omega)(1) = 0, \end{aligned}$$

with η determined from the second equation in (1.11), and

$$(1.15) \quad \varepsilon \eta_{xx} = \lambda \eta \quad \text{with} \quad \eta_x(0) = \eta(1) = 0,$$

with ω identically equal to zero. The second of these problems, (1.15), is exactly solvable and describes the diffusive behavior of the nutrient in the absence of phytoplankton. Thus, it is not directly linked to the phytoplankton bifurcation problem that we consider, and we will not discuss it further. The phytoplankton behavior that we focus on is described by (1.14) instead, and hence we have returned to a scalar system as studied in [5, 7, 8, 10, 12, 14, 15]. However, our viewpoint differs significantly from that of those studies. The simulations in [11] (and section 3 of the present article) suggest that the destabilization of $(\bar{\omega}, \bar{\eta})$ into a DCM is merely the first in a series of bifurcations. In fact, section 3 shows that this DCM undergoes “almost immediately” a second bifurcation of Hopf type; i.e., it begins to oscillate periodically in time. According to [14], this is impossible in a scalar model (also, it has not been numerically observed in such models), and so the Hopf bifurcation must be induced by the *weak* coupling between ω and η in the full model (1.5).

Our analysis establishes that the largest eigenvalue λ_0 of (1.14) which induces the (stationary) DCM as it crosses through zero is the first of a sequence of eigenvalues λ_n that are only $\mathcal{O}(\varepsilon^{1/3})$ apart (see Figure 3.3, where $\varepsilon^{1/3} \approx 0.045$). The simulations in section 3 show that the distance between this bifurcation and the subsequent Hopf bifurcation of the DCM is of the same magnitude; see Figure 3.3 especially. Thus, the stationary DCM already destabilizes while λ_0 is still asymptotically small in ε , which indicates that the amplitude of the bifurcating DCM is also still asymptotically small and determined (at leading order) by $\omega_0(x)$, the eigenfunction associated with λ_0 . This agrees fully with our linear stability analysis, since $\omega_0(x)$ indeed has the structure of a DCM (see sections 2 and 7). As a consequence, the *leading order* (in ε) stability analysis of the DCM is also governed by the partially decoupled system (1.11). In other words, although what drives the secondary bifurcation(s) is the

coupling between $\omega(x)$ and $\eta(x)$ in (1.5), the leading order analysis is governed by the eigenvalues and eigenfunctions of (1.14). Naturally, the next eigenvalues and their associated eigenfunctions will play a key role in such a secondary bifurcation analysis, as will the eigenvalues and eigenfunctions of the trivial system (1.15).

Therefore, a detailed knowledge of the nature of the eigenvalues and eigenfunctions of (1.14) forms the foundation of analytical insight in the bifurcations exhibited by (1.5). This is the topic of the present paper; the subsequent (weakly) nonlinear analysis is the subject of work in progress.

The structure of the eigenvalue problem (1.14) is rather subtle, and therefore we employ two different analytical approaches. In sections 4–6, we derive explicit and rigorous bounds on the eigenvalues in terms of expressions based on the zeroes of the Airy function of the first kind and its derivative; see Theorem 2.1. We supplement this analysis with a WKB approach in section 7, where we show that the critical eigenfunctions have the structures of a DCM or a BL. This analysis establishes the existence of, first, the aforementioned sequence of eigenvalues that are $\mathcal{O}(\varepsilon^{1/3})$ apart, which is associated with the bifurcation of a DCM; and second, of another eigenvalue which also appears for biologically relevant parameter combinations and which is associated with the bifurcation of a BL—this bifurcation was not observed in [11]. This eigenvalue is isolated, in the sense that it is not part of the eigenvalue sequence associated with the DCMs—instead, it corresponds to a zero of a linear combination of the Airy function of the second kind and its derivative. Depending on the value of the dimensionless parameter a , the trivial state $(\bar{\omega}, \bar{\eta})$ bifurcates either into a DCM or into a BL. Our analysis establishes the bifurcation sets explicitly in terms of the parameters in the problem (section 2.2) and is confirmed by numerical simulations (section 3). Note that the codimension 2 point, at which DCM- and BL-patterns bifurcate simultaneously and which we determine explicitly, is related to that studied in [20]. Nevertheless, the differences are crucial—for instance, [20] considers a two-layer ODE model where, additionally, the DCM interacts with an SL instead of a BL (an SL cannot occur in our setting because $V > 0$ in (1.1); see Remark 1.1).

The outcome of our analysis is summarized in section 2, in which we also summarize the bio-mathematical interpretations of this analysis. We test and challenge the results of the stability analysis by numerical simulations of the full model in section 3. Although our insights are based only on linear predictions, and we do not yet have analytical results on the (nonlinear) stability of the patterns that bifurcate, we do find that there is an excellent agreement between the linear analysis and the numerical simulations. Thus, our analysis of (1.14) yields explicit bifurcation curves in the biological parameter space associated with (1.1). For any given values of the parameters, our analysis predicts whether one may expect a phytoplankton pattern with the structure of a (possibly oscillating) DCM, a pattern with the structure of a BL, or whether the phytoplankton will become extinct. Moreover, we also briefly consider secondary bifurcations into time-periodic patterns. These bifurcations are not directly covered by our linear analysis, but the distance between the first and second bifurcation in parameter space implies that the linearized system (1.14) must play a crucial role in the subsequent (weakly) nonlinear analysis; see the discussion above.

Remark 1.1. Our approach and findings for the model (1.1) (equivalently, (1.5)) are also applicable and relevant for more extensive models:

- In [11], (1.1) was extended to a model for various phytoplankton species $W_i(z, t)$ ($i = 1, \dots, n$). A stability analysis of the trivial pattern $W_i \equiv 0$, $N \equiv N_B$ yields n uncoupled copies of (1.14) in which the parameters depend on the species, i.e., on

the index i . As a consequence, the results of this paper can also be applied to this multispecies setting.

- It is natural to include the possibility of horizontal flow and diffusion in the model (1.1). In the most simple setting, this can be done by allowing W and N to vary with (x, y, z, t) and to include horizontal diffusion terms in (1.1), i.e., $D_H(W_{xx} + W_{yy})$ and $D_H(N_{xx} + N_{yy})$ with $D_H \neq D$, in general—see [17], for instance. Again, the linear stability analysis of the trivial state is essentially not influenced by this extension. The exponentials in the ansatz following (1.10) now need to be replaced by $\exp(\lambda\tau + i(k_x\tilde{x} + k_y\tilde{y}))$, where k_x and k_y are wave numbers in the (rescaled) x and y directions. As a consequence, one only has to replace ℓ by $\ell - D_H(k_x^2 + k_y^2)$ in (1.14).

- The fact that we assign specific formulas to the growth and light intensity functions $P(L, N)$ (see (1.3)) and $L(z, t)$ (see (1.2)) is inessential for our analysis. One needs only that $f(x)$ is *decreasing* and *bounded* in $[0, 1]$ —both assumptions are natural from a biological standpoint.

- We have considered “sinking” phytoplankton species in our model, i.e., $V > 0$ in (1.1) and thus $a > 0$ in (1.14). Our analysis can also be applied to buoyant species ($V \leq 0$). In that case, the bifurcating DCMs may transform into SLs—see also [10, 15].

- The values of ε , a , and ℓ in (1.9) are typical of oceanic settings [11]. These values differ in an estuary, and ε can no longer be assumed to be asymptotically small; see [19] and the references therein. Moreover, phytoplankton blooms in an estuary are strongly influenced by the concentration of suspended sediment and typically occur not only at a certain depth z , but also at a certain horizontal position in the estuary. Thus, (1.14) must be extended to account for such blooms; however, it may still play an important role as a limiting case or a benchmark [19].

2. The main results. In the first part of this section, we present our main results in full mathematical detail. In section 2.2, we present a bio-mathematical interpretation of these results.

2.1. Mathematical analysis. We define the parameter $\nu = 1/(1 + \eta_H)$, the function F through

$$(2.1) \quad F(x) = F(x; j_H, \kappa, \nu) = f(0) - f(x) \geq 0 \quad \text{for all } x \in [0, 1]$$

(see (1.13)), and the constants $\sigma_L = \sigma_L(\kappa, j_H, \nu)$ and $\sigma_U = \sigma_U(\kappa, j_H, \nu)$ so that

$$(2.2) \quad \sigma_L x \leq F(x) \leq \sigma_U x \quad \text{for all } x \in [0, 1].$$

The optimal values of σ_U and σ_L can be determined explicitly. This (simple yet technical) analysis is postponed until after the formulation of Theorem 2.1; see Lemma 2.1 and Figures 2.2 and 2.3. Next, we define the parameters

$$(2.3) \quad A = \frac{a^2}{4}, \quad \beta = \sqrt{\frac{A}{\sigma}}, \quad \text{and} \quad 0 < \gamma \equiv \left(\frac{\varepsilon}{\sigma}\right)^{1/3} \ll 1,$$

with a as in (1.7) and σ an a priori parameter. (Later, σ will be set equal to either σ_L or σ_U .) Furthermore, we write Ai and Bi for the Airy functions of the first and second kind [1], respectively, and $A_n < 0$, $n \in \mathbf{N}$, for the n th zero of $\text{Ai}(x)$; see Figure 2.1. We also define the functions

$$(2.4) \quad \Gamma(\text{Ai}, x) = \text{Ai}(x) - \sqrt{\gamma}\beta^{-1}\text{Ai}'(x) \quad \text{and} \quad \Gamma(\text{Bi}, x) = \text{Bi}(x) - \sqrt{\gamma}\beta^{-1}\text{Bi}'(x)$$

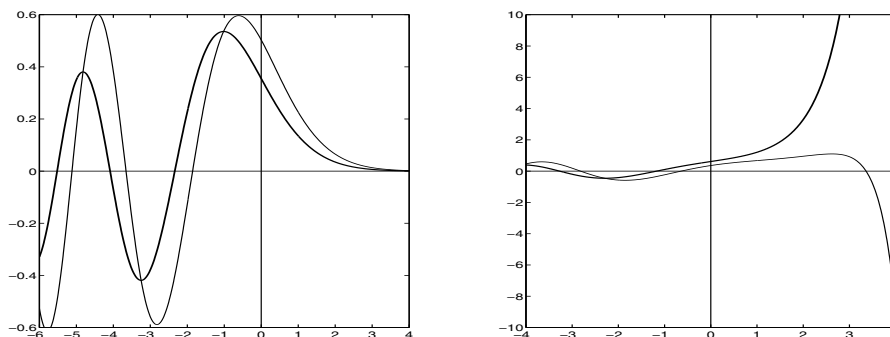


FIG. 2.1. Left: Airy function of the first kind (thick line) plotted with the function $\Gamma(\text{Ai}, \cdot)$ (thin line). Right: Airy function of the second kind (thick line) plotted with $\Gamma(\text{Bi}, \cdot)$ (thin line). Here, $\varepsilon = 0.1$, $a = 3$, and $\sigma = 2$.

(see Figure 2.1 and section 5.1) and write $A'_{n,\sigma}$ for the n th zero of $\Gamma(\text{Ai}, x)$ ($n \in \mathbf{N}$)—which is $\mathcal{O}(\sqrt{\gamma})$ close to A_n —and $B_{0,\sigma}$ for the positive zero of $\Gamma(\text{Bi}, \gamma^{-1}(1+x))$ —which exists for all $\beta > 1$ and is equal to $\beta^2 - 1$ at leading order in γ ; see Lemma A.2 for more accurate estimates. Finally, we let

$$(2.5) \quad \lambda^* = f(0) - \ell - A, \quad \lambda_0^{*,\sigma} = \lambda^* + A\beta^{-2}B_{0,\sigma}, \quad \lambda_n^{*,\sigma} = \lambda^* - \gamma A\beta^{-2}|A'_{n,\sigma}|, \quad n \in \mathbf{N},$$

and we note that $\lambda_0^{*,\sigma}$ and $\lambda_n^{*,\sigma}$ are decreasing functions of σ . We can now formulate our main result.

THEOREM 2.1. *Let $M \in \mathbf{N}$. There exists an $\varepsilon_0 > 0$ and a constant $C > 0$ such that, for all $0 < \varepsilon < \varepsilon_0$ and $0 \leq n \leq M$, the first $M+1$ eigenvalues $\lambda_0 > \dots > \lambda_M$ of (1.14) satisfy the following:*

(a) *For each $0 < \sigma_U < A$, there exists a constant $B > 0$ such that*

$$\lambda_0^{*,\sigma_U} - C\varepsilon^{2/3}e^{-B/\sqrt{\varepsilon}} \leq \lambda_0 \leq \lambda_0^{*,\sigma_L} + C\varepsilon^{2/3}e^{-B/\sqrt{\varepsilon}}$$

and

$$\lambda_n^{*,\sigma_U} - C\varepsilon^{1/6}e^{-B/\sqrt{\varepsilon}} \leq \lambda_n \leq \lambda_n^{*,\sigma_L} + C\varepsilon^{1/6}e^{-B/\sqrt{\varepsilon}} \quad \text{for all } 1 \leq n \leq M.$$

(b) *For each $\sigma_L > A$, there exists a constant $B > 0$ such that*

$$\lambda_{n+1}^{*,\sigma_U} - C\varepsilon^{1/6}e^{-B/\sqrt{\varepsilon}} \leq \lambda_n \leq \lambda_{n+1}^{*,\sigma_L} + C\varepsilon^{1/6}e^{-B/\sqrt{\varepsilon}} \quad \text{for all } 0 \leq n \leq M.$$

Theorem 2.1 and (2.5) establish that, for any $M \in \mathbf{N}$ and for sufficiently small $\varepsilon > 0$ (equivalently, for sufficiently small $\gamma > 0$), all first $M+1$ eigenvalues of (1.14) are $\mathcal{O}(\varepsilon^{1/3})$ close to λ^* , except for the special eigenvalue λ_0 if $\sigma_U < A$. Both types of eigenvalues correspond to biologically relevant patterns in (1.1)—to DCMs and BLs, respectively; see section 2.2. This dependence on the parameters is quite subtle; further, the weakly nonlinear stability analysis must be based on a detailed understanding of the linear eigenvalue problem including all of the eigenmodes associated with the asymptotically close eigenvalues (see also the introduction). As a result, the required analysis becomes rather extensive. For this reason, we defer the proof of Theorem 2.1 to sections 4–6.

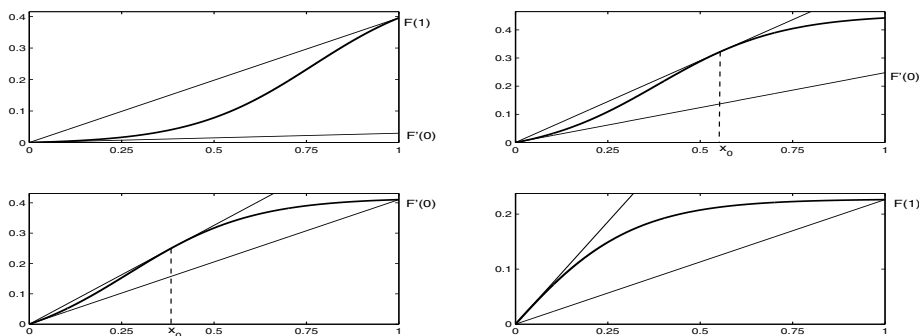


FIG. 2.2. The function F (thick curve) and the linear functions bounding it (thin lines). Here, $\eta_H = 1$, $\kappa = 6$, and $j_H = 0.01 < j_H^{(1)}$ (top left panel), $j_H^{(1)} < j_H = 0.1 < j_H^{(2)}$ (top right panel), $j_H^{(2)} < j_H = 0.2 < 1$ (bottom left panel), and $j_H = 1.2 > 1$ (bottom right panel).

Moreover, this analysis establishes that the bounds on the eigenvalues are, up to exponentially small terms, explicitly given in terms of zeroes of the Airy functions $\text{Ai}(x)$ and $\text{Bi}(x)$ (and their derivatives (2.4)) and of the bounds $\sigma_L x$ and $\sigma_U x$ on $F(x)$ in (2.2). This enables us (by unscaling) to explicitly quantify the regions in the parameter space associated with (1.1) in which DCMs or BLs can be expected to appear (see sections 2.2 and 3).

The following lemma provides explicit control on $\sigma_L x$ and $\sigma_U x$.

LEMMA 2.1. *Let*

$$j_H^{(1)}(\kappa) = \frac{e^{-\kappa} - 1 + \kappa}{e^{\kappa} - 1 - \kappa} \quad \text{and} \quad j_H^{(2)}(\kappa) = \frac{e^{-\kappa}}{j_H^{(1)}(\kappa)},$$

so that $0 < j_H^{(1)}(\kappa) < j_H^{(2)}(\kappa) < 1$ for all $\kappa > 0$. Also, for all $\kappa > 0$ and $j_H \in (j_H^{(1)}(\kappa), 1)$, define the point $x_0 = x_0(\kappa, j_H) \in (0, 1)$ via $F(x_0) = x_0 F'(x_0)$. Then,

$$(2.6) \quad \sigma_L = \begin{cases} F'(0), & 0 < j_H \leq j_H^{(2)}, \\ F(1), & j_H > j_H^{(2)}, \end{cases} \quad \sigma_U = \begin{cases} F(1), & 0 < j_H \leq j_H^{(1)}, \\ F'(x_0), & j_H^{(1)} < j_H < 1, \\ F'(0), & j_H \geq 1, \end{cases}$$

and

$$(2.7) \quad \sigma_L(\kappa, j_H, \nu) = \nu \sigma_L(\kappa, j_H, 1), \quad \sigma_U(\kappa, j_H, \nu) = \nu \sigma_U(\kappa, j_H, 1).$$

This lemma is proved by straightforward calculus. Figures 2.2 and 2.3 give a graphical representation of the lemma for various representative subcases.

As we shall see in section 3, the eigenvalue bounds established in Theorem 2.1 are quite sharp and predict very well the bifurcations of the full unscaled model (1.1). Nevertheless, the rigorous analysis of sections 4–6 yields no information on the characteristics of the associated eigenfunctions, which are of particular interest to the nature of the patterns generated by (1.1) as λ_0 crosses through zero (see section 3). Moreover, the width of the intervals bounding the eigenvalues of (1.14) is of the same order in ε —namely of $\mathcal{O}(\varepsilon^{1/3})$ —as the distance between successive eigenvalues. This

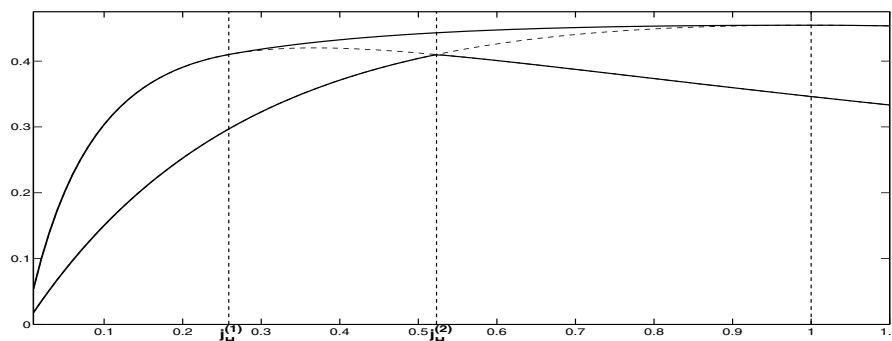


FIG. 2.3. The quantities σ_U (upper thick curve), σ_L (lower thick curve), $F(1)$ (dashed curve to the left), and $F'(0)$ (dashed curve to the right) as functions of j_H and for $\eta_H = 0.1$, $\kappa = 2$. Note that $F(1)$ merges with σ_U for $j_H \leq j_H^{(1)}$ and with σ_L for $j_H \geq j_H^{(2)}$, while $F'(0)$ merges with σ_L for $j_H \leq j_H^{(2)}$ and with σ_U for $j_H \geq 1$. Also note that the WKB method (see section 7) yields that the location of the eigenvalue close to $\lambda_0^{*,\sigma}$ (see Theorem 2.1) is determined by $F(1)$, at leading order, whereas the locations of the eigenvalues close to $\lambda_n^{*,\sigma}$, $n \in \mathbf{N}$, are determined by $F'(0)$ at leading order.

is especially relevant in the transitional case $\sigma_L < A < \sigma_U$, for which Theorem 2.1 offers no information.

For these reasons, we complete our analysis of (1.14) with an asymptotic WKB approximation (section 7). We derive asymptotic formulas for the eigenvalues and for the corresponding eigenfunctions. Using these formulas, we show the following:

- In case (a) of Theorem 2.1, the profile of the eigenfunction ω_0 corresponding to the largest eigenvalue λ_0 is of boundary layer type near the bottom. In terms of the phytoplankton concentration, this profile corresponds to a BL.
- In case (b) of the same theorem, ω_0 has the shape of a spike around the point $x = x_{\text{DCM}}$, where x_{DCM} is determined, to leading order in ε , by $F(x_{\text{DCM}}) = A$ (see Figure 7.1). This profile corresponds to a DCM around x_{DCM} .
- The transitional region between cases (a) and (b) in Theorem 2.1 is described, to leading order in ε , by the equation $A = F(1)$. Indeed, the leading order approximation to λ_0 is

(2.8)

$$\lambda_{0,0} = f(1) - \ell \quad \text{in the region } F(1) = f(0) - f(1) < A \text{ (and } \omega_0 \text{ is a BL),}$$

(2.9)

$$\lambda_{0,0} = \lambda^* = f(0) - \ell - A \quad \text{in the region } F(1) = f(0) - f(1) > A \text{ (and } \omega_0 \text{ is a DCM).}$$

Recalling Lemma 2.1, we see that this transition occurs at a value of A which is, to leading order in ε , equal to σ_U when $0 < j_H \leq j_H^{(1)}$, equal to σ_L when $j_H \geq j_H^{(2)}$, and between σ_U and σ_L when $j_H^{(1)} < j_H < j_H^{(2)}$.

2.2. Bio-mathematical interpretation. The agreement between the numerical simulations and the field data reported in [11] establishes the biological relevance of model problem (1.1) and of its dynamics. This paper contains the first steps towards a bio-mathematical understanding of this model, especially in relation to the existing models in the literature that exhibit only simple, stationary patterns [5, 7, 8, 10, 12, 14].

The fact that (1.1) can be scaled into the singularly perturbed equation (1.5) for biologically relevant choices of the parameters is essential to the analysis in this paper. Moreover, together with the linear stability analysis, these scalings enable us to understand the fundamental structure of the twelve-dimensional parameter space associated with (1.1) and its boundary conditions (1.4) (in the biologically relevant region). In fact, it follows from Theorem 2.1 and (2.8)–(2.9) that the dimensionless parameters A , ℓ , $f(0)$, and $f(1)$, which are defined in section 2.1, are the main parameter combinations in the model as they capture its most relevant biological aspects.

Our stability analysis determines the regions in parameter space in which phytoplankton may persist, i.e., in which the trivial solution of (1.1) and (1.4) corresponding to absence of phytoplankton ($W(z, t) \equiv 0$ in (1.1)) is unstable. In that case, nontrivial patterns with $W(z, t) > 0$, for all t , bifurcate from the trivial solution, which implies that the model admits stable, positive phytoplankton populations. Theorem 2.1 establishes the existence of two distinct types of phytoplankton populations at onset. One is formed by a large—in fact infinite—family of “DCM-modes” and occurs for A below the threshold value $f(0) - f(1)$; the region where these modes become stable is determined by $\lambda^* = f(0) - \ell - A$; see (2.9). Within this family, the phytoplankton concentrations are negligible for most z , except for a certain localized (spatial) region in which the phytoplankton population is concentrated—see Figure 7.1 in which the first, most unstable member of this family is plotted (in scaled coordinates). These are the DCM-patterns observed in [11]. Our analysis shows that many different DCM-patterns appear almost instantaneously. More precisely, as a parameter enters into the region in which the trivial solution is unstable, a succession of asymptotically close bifurcations in which different types of DCM-patterns are created takes place. In other words, even asymptotically close to onset, there are many competing DCM-modes. This partly explains why the “pure” DCM-mode as represented in Figure 7.1 can be observed only very close to onset (see [11] and section 3.2): it may be destabilized by the competition with other modes.

The second type of phytoplankton population that may appear at onset occurs for A above the threshold value $f(0) - f(1)$ and has the structure of a BL: the phytoplankton population is concentrated near $z = z_B$, i.e., at the bottom of the water column. Unlike the DCM-modes, there is a *single* BL-mode; the region where this mode becomes stable is determined, in this case, by $f(1) - \ell$; see (2.8). This mode may also dominate the dynamics of (1.1) in a part of the biologically relevant parameter space, as may be seen in section 3.2. Note that the BL-mode has not been observed in [11]; naturally, this is hardly surprising since one can sample numerically only a very limited region of a twelve-dimensional parameter space. From the biological point of view, the fact that the model (1.1) allows for attractors of the BL type may be the most important finding of this paper. Like DCMs, BLs have been observed in field data (see [15] and references therein). The analysis here quantifies the parameter values for which DCM- or BL-patterns occur. Hence, our results may be used to determine oceanic regions and/or phytoplankton species for which BLs may be expected to exist. It would be even more interesting to locate a setting in which DCMs and BLs interact, as they are expected to do because of the existence of the codimension 2 point at which the (first) DCM-mode and the BL-mode bifurcate simultaneously; see section 3.

3. Bifurcations and simulations.

3.1. The bifurcation diagram. In this section, we use the WKB expressions (2.8)–(2.9) for the first few eigenvalues to identify the bifurcations that system (1.14) undergoes. In this way, we identify the regions in the parameter space where the BL

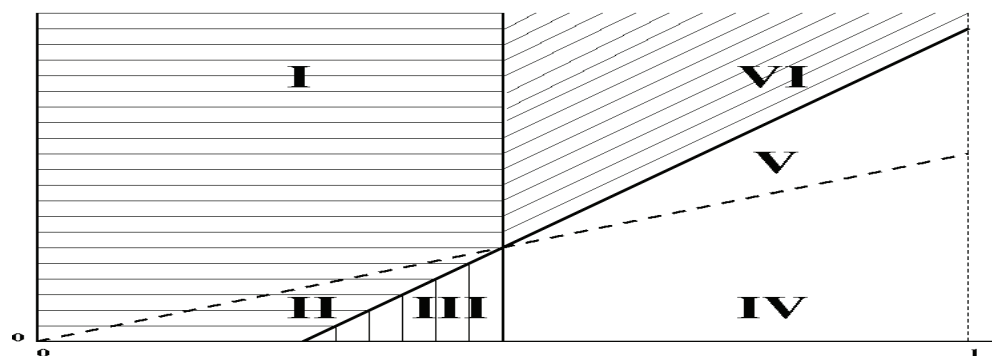


FIG. 3.1. The bifurcation diagram in the (ν, A) -plane. The horizontal axis corresponds to $\nu = 1/(1 + \eta_H)$, while the vertical one corresponds to $A = a^2/4$. In the region shaded horizontally, the trivial zero state is stable. In the region shaded vertically, DCMs bifurcate, while BL profiles remain damped. In the region shaded diagonally, BL profiles bifurcate, while DCM profiles remain damped. Finally, in the unshaded region, both profiles grow linearly.

and DCM steady states become stable. As already mentioned in the Introduction, we are primarily interested in the effect of environmental conditions—in particular, of nutrient concentration and diffusion—on phytoplankton. For this reason, we choose to vary the parameters $\eta_H = N_H/N_B$ (which encapsulates information pertaining to the nutrient levels and nutrient absorption by phytoplankton) and $a = V/\sqrt{\mu D}$ (which is a measure of diffusion; see (1.7)). The remaining four dimensionless parameters (ε , κ , j_H , and ℓ) are kept constant. We recall here the definitions $\nu = 1/(1 + \eta_H)$ and $A = a^2/4$.

The curves separating the regions in the (ν, A) -plane which are characterized by qualitatively different behavior of the rescaled model (1.5), (1.8) may be found by recasting (2.9) and (2.8) in terms of the rescaled parameters. In particular, using (1.13), (2.1), and (2.5), we find (see Figure 3.1) the following:

- In regions I and II, λ_0 is given, to leading order, by (2.8) (in region I) and by (2.9) (in region II). In either case, $\lambda_0 < 0$, and hence the zero (trivial) state is stable.
- In region III, λ_0 is given by (2.9) and is positive. In fact, the further into this region one goes, the more eigenvalues cross zero and become positive, since they are $\mathcal{O}(\varepsilon^{1/3})$ apart by Theorem 2.1. All of these eigenvalues are associated with DCMs.
- In region VI, λ_0 is given by (2.8) and is positive, while all other eigenvalues are negative. Thus, the only bifurcating patterns in this regime are BL profiles.
- Finally, in regions IV and V, eigenvalues associated with both BL and DCM profiles are positive, and thus no further info can be derived from our linear analysis.

The boundaries of these regions may be deduced explicitly in the aforementioned manner. First, setting the expression for λ_0 in (2.8) equal to zero, we obtain, to leading order, the vertical line separating the regions I, II, and III from the regions IV, V, and VI,

$$\nu = \ell(1 + e^\kappa j_H).$$

Next, setting the expression for λ_0 in (2.9) equal to zero, we obtain, to leading order, the diagonal line separating the regions I, II, and VI from III, IV, and V,

$$A = \frac{1}{1 + j_H} \nu - \ell.$$

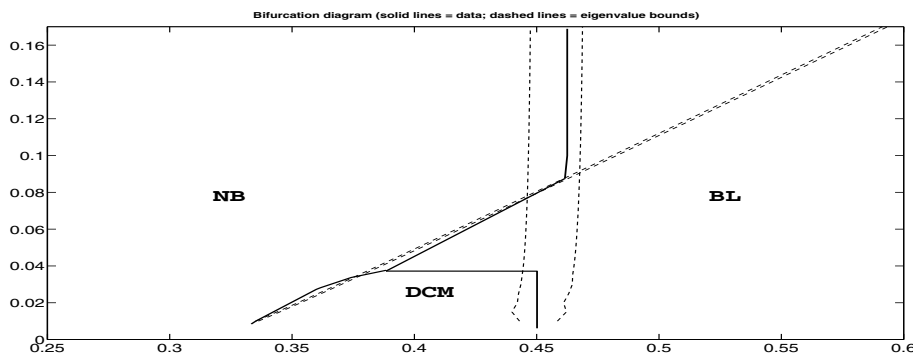


FIG. 3.2. The bifurcation diagram in the (ν, A) -plane for $\varepsilon = 9 \cdot 10^{-5}$, $\ell = 0.2$, $j_H = 0.5$, $\kappa = 1$. (“NB” stands for “no blooming.”) The solid curves correspond to numerical simulations, while the dashed ones correspond to the bounds predicted theoretically; see Theorem 2.1.

Finally, setting the expressions for λ_0 in (2.8) and (2.9) equal to each other, we obtain the transitional regime $A = F(1)$. In terms of the rescaled parameters, we find

$$A = \left(\frac{1}{1 + j_H} - \frac{1}{1 + e^\kappa j_H} \right) \nu.$$

Since the physical region $n_H > 0$ corresponds to the region $0 < \nu < 1$, these formulas imply that

- (a) for $0 < \ell < (1 + e^\kappa j_H)^{-1}$, both a BL and a DCM may bifurcate,
- (b) for $(1 + e^\kappa j_H)^{-1} < \ell < (1 + j_H)^{-1}$, only a DCM may bifurcate,
- (c) for $\ell > (1 + j_H)^{-1}$, the trivial state is stable.

Remark 3.1. Similar information may be derived by the rigorous bounds in Theorem 2.1, with the important difference that the dividing curves have to be replaced by regions of finite thickness.

3.2. Numerical simulations. In this section, we present numerical simulations on the full model (1.1)–(1.4), and we compare the results with our theoretical predictions. The parameters are chosen in biologically relevant regions [11].

We considered first the validity of our asymptotic analysis; i.e., we checked whether the analytically obtained bounds for the occurrence of the DCMs and BLs—see Theorem 2.1, section 3.1, Figure 3.1, and Remark 3.1—can be recovered by numerical simulations of the PDE (1.1)–(1.4). We used the numerical method described in Remark 3.2 at each node of a two-dimensional grid of a part of the (ν, A) -parameter plane (keeping all other parameters fixed) to determine the attracting pattern generated by (1.1)–(1.4) and chose the initial profile at each node in the parameter space to be the numerically converged pattern for an adjacent node at the previous step.

In Figure 3.2, we present the region near the codimension 2 point in the (ν, A) -parameter plane at which both the DCMs and the BLs bifurcate (with all other parameters fixed: $\varepsilon = 9 \cdot 10^{-5}$, $\ell = 0.2$, $j_H = 0.5$, $\kappa = 1$). Away from this codimension 2 point, the numerically determined bifurcation curves are clearly within the bounds given by Theorem 2.1 and thus confirm our analysis. Note that this suggests that the bifurcations have a supercritical nature—an observation that does not follow from our linear analysis. Near the codimension 2 point, a slight discrepancy between

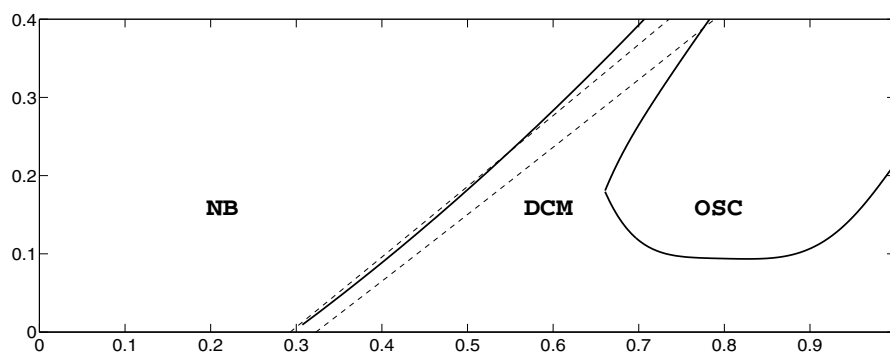


FIG. 3.3. The bifurcation diagram in the (ν, A) -plane for $\varepsilon = 9 \cdot 10^{-5}$, $\ell = 0.25$, $j_H = 0.033$, $\kappa = 20$. Region NB corresponds to no blooming, and region OSC to oscillatory DCMs. The solid curves correspond to numerical simulations, and the dashed ones to the points at which λ_0 (left line) and λ_1 (right line) cross zero; see (2.9) and Figure 3.1. For these parameter values, the bifurcation of the BLs occurs in a nonphysical part of the domain.

our analysis and the numerical findings becomes apparent. First, we note that the bifurcation from the trivial state (no phytoplankton) to the DCM state is not exactly in the region determined by Theorem 2.1. However, for this combination of parameters, this region is quite narrow—in fact, it is narrower than the width of the rectangular grid of the (ν, A) -parameter plane that we used to determine Figure 3.2, which implies that the simulations do not disagree with the analysis. The other discrepancy, namely the occurrence of a small “triangle” of BL patterns in the region where one would expect DCMs, is related to the presence of the codimension 2 point. To understand the true nature of the dynamics, one needs to perform a weakly nonlinear analysis near this point and, presumably, a more detailed numerical analysis that distinguishes between DCMs, BLs, and patterns that have the structure of a combined DCM and BL. This is the topic of work in progress.

Unlike the simulations presented in [11], here we considered the secondary bifurcations only briefly. Figure 3.3 shows the primary bifurcation of the trivial state into a DCM and the secondary bifurcation (of Hopf type) of the DCM into an oscillating DCM—see [11] for more (biological) details on this behavior. A priori, one would expect that our linear stability analysis of the trivial state could not cover this Hopf bifurcation. However, in Figure 3.3 we also plotted the leading order approximations of the curves at which the first two eigenvalues associated with the stability of the trivial state, λ_0 and λ_1 , cross through the imaginary axis. It follows that the distance (in parameter space) between the primary and the secondary bifurcations is asymptotically small in ε , and similar to the distance between the successive eigenvalues λ_n . This observation is based on several simulations realized for different values of ε . It is crucial information for the subsequent (weakly) nonlinear analysis, since the fact that the DCM undergoes its secondary Hopf bifurcation for parameter combinations that are asymptotically close (in ε) to the primary bifurcation implies that the above a priori expectation is not correct; instead, the stability and bifurcation analysis of the DCM can, indeed, be based on the linear analysis presented here. The higher order eigenvalues $\lambda_1, \lambda_2, \dots$, the associated eigenfunctions $\omega_1(x), \omega_2(x), \dots$, and their “slaved” η -components $\eta_1(x), \eta_2(x), \dots$ (which can be determined explicitly using (1.11)) will serve as necessary inputs for this nonlinear analysis.

Thus, a “full” linear stability analysis of the uncoupled system (1.14) as presented here may serve as a foundation for the analysis of secondary bifurcations that can only occur in the coupled system (see the introduction and [14]). This feature is very special and quite uncommon in explicit models. It is due to the *natural singularly perturbed nature* of the scaled system (1.5), and it provides an opportunity to obtain fundamental insight into phytoplankton dynamics. This analysis, including the aforementioned codimension 2 analysis and the associated secondary bifurcations of BLs, is the topic of work in progress.

Remark 3.2. The numerical results were obtained by the “Method of Lines” approach. First, we discretized the spatial derivatives approximating the diffusion terms in the model using second-order symmetric formulas and employing a third-order upwind-biased method to discretize the advection term (see [13] for the suitability of these schemes to the current problem). Next, we integrated the resulting system of ODEs forward in time with the widely used time-integration code VODE (see [3] and <http://www.netlib.org/ode>). Throughout all simulations, we combined a spatial grid of a sufficiently high resolution with a high precision time integration to ensure that the conclusions drawn from the simulations are essentially free of numerical errors.

4. Eigenvalue bounds. As a first step towards the proof of Theorem 2.1, we recast (1.14) in a form more amenable to analysis. First, we observe that the operator involved in this eigenvalue problem is self-adjoint only if $a = 0$. Applying the Liouville transformation

$$(4.1) \quad w(x) = e^{-\sqrt{A/\varepsilon}x} \omega(x) = e^{-(\beta/\gamma^{3/2})x} \omega(x),$$

we obtain the self-adjoint problem

$$\begin{aligned} \varepsilon w_{xx} + (f(x) - \ell - A)w &= \lambda w, \\ \left(\sqrt{\varepsilon} w_x - \sqrt{A} w\right)(0) &= \left(\sqrt{\varepsilon} w_x - \sqrt{A} w\right)(1) = 0. \end{aligned}$$

Recalling (2.1) and (2.5), we write this equation in the form

$$(4.2) \quad \mathcal{L}w = \mu w, \quad \text{with} \quad \mathcal{G}(w, 0) = \mathcal{G}(w, 1) = 0.$$

The operator \mathcal{L} , the scalar μ , and the linear functionals $\mathcal{G}(\cdot, x)$ are defined by

$$(4.3) \quad \mathcal{L} = -\varepsilon \frac{d^2}{dx^2} + F(x), \quad \mu = \lambda^* - \lambda, \quad \mathcal{G}(w, x) = w(x) - \sqrt{\frac{\varepsilon}{A}} w_x(x).$$

This is the desired form of the eigenvalue problem (1.14). To prove Theorem 2.1, we decompose the operator \mathcal{L} into a self-adjoint part for which the eigenvalue problem is exactly solvable and a positive definite part. Then, we use the following comparison principle to obtain the desired bounds.

THEOREM 4.1 (see [18, sections 8.12–8.13]). *Let $\hat{\mathcal{A}}$ and \mathcal{A} be self-adjoint operators bounded below with compact inverses, and write their eigenvalues as $\hat{\mu}_0 \leq \hat{\mu}_1 \leq \dots \leq \hat{\mu}_n \leq \dots$ and $\mu_0 \leq \mu_1 \leq \dots \leq \mu_n \leq \dots$, respectively. If $\mathcal{A} - \hat{\mathcal{A}}$ is positive semidefinite, then $\hat{\mu}_n \leq \mu_n$ for all $n \in \{0, 1, \dots\}$.*

4.1. Crude bounds for the eigenvalues of \mathcal{L} . First, we derive crude bounds for the spectrum $\{\mu_n\}$ of \mathcal{L} to demonstrate the method and establish that \mathcal{L} satisfies the boundedness condition of Theorem 4.1.

LEMMA 4.1. *The eigenvalues μ_n satisfy the inequalities*

$$(4.4) \quad -A \leq \mu_0 \leq F(1) - A \quad \text{and} \quad \varepsilon n^2 \pi^2 \leq \mu_n \leq F(1) + \varepsilon n^2 \pi^2, \quad n \in \mathbf{N}.$$

Proof. Let $c \in \mathbf{R}$. We start by decomposing \mathcal{L} as

$$(4.5) \quad \mathcal{L} = \mathcal{L}^{0,c} + \mathcal{F}^{0,c}, \quad \text{where} \quad \mathcal{L}^{0,c} = -\varepsilon \frac{d^2}{dx^2} + c \quad \text{and} \quad \mathcal{F}^{0,c} = F(x) - c.$$

Then, we write $\{\mu_n^{0,c}\}$ for the set of eigenvalues of the problem

$$(4.6) \quad \mathcal{L}^{0,c} w^{0,c} = \mu_n^{0,c} w^{0,c}, \quad \text{with} \quad \mathcal{G}(w^{0,c}, 0) = \mathcal{G}(w^{0,c}, 1) = 0,$$

with the eigenvalues arranged so that $\mu_0^{0,c} \leq \mu_1^{0,c} \leq \dots \leq \mu_n^{0,c} \leq \dots$.

For $c = c_L = 0$, the operator \mathcal{L}^{0,c_L} is self-adjoint, while $\mathcal{F}^{0,c_L} = F(x) \geq 0$ is a positive definite multiplicative operator. Thus, using Theorem 4.1, we obtain the inequalities

$$(4.7) \quad \mu_n^{0,c_L} \leq \mu_n \quad \text{for all} \quad n \in \mathbf{N} \cup \{0\}.$$

Next, for $c = c_U = F(1)$, the operator $\mathcal{F}^{0,c_U} = F(x) - F(1) \leq 0$ is negative definite, while \mathcal{L}^{0,c_U} is self-adjoint. Hence, we may write

$$\mathcal{L}^{0,c_U} = \mathcal{L} - \mathcal{F}^{0,c_U},$$

where $-\mathcal{F}^{0,c_U}$ is now positive definite. The fact that the spectrum $\{\mu_n\}$ of \mathcal{L} is bounded from below by (4.7) allows us to use Theorem 4.1 to bound each μ_n from above,

$$\mu_n \leq \mu_n^{0,c_U} \quad \text{for all} \quad n \in \mathbf{N} \cup \{0\}.$$

Combining this bound and (4.7), we obtain

$$(4.8) \quad \mu_n^{0,c_L} \leq \mu_n \leq \mu_n^{0,c_U} \quad \text{for all} \quad n \in \mathbf{N} \cup \{0\}.$$

Naturally, the eigenvalue problem (4.6) may be solved exactly to obtain

$$(4.9) \quad \mu_0^{0,c} = c - A \quad \text{and} \quad \mu_n^{0,c} = c + \varepsilon n^2 \pi^2, \quad n \in \mathbf{N}.$$

Combining these formulas with (4.8), we obtain the inequalities (4.4). \square

4.2. Tight bounds for the eigenvalues of \mathcal{L} . The accurate bounds for the eigenvalues of (4.2) described in Theorem 2.1 may be obtained by bounding F by linear functions; see (2.2) and Lemma 2.1. In the next lemma, we bound the eigenvalues μ_n by the eigenvalues $\mu_n^{1,\sigma}$ of a simpler problem. Then, in Lemma 4.3, we obtain strict, exponentially small bounds for $\mu_n^{1,\sigma}$.

LEMMA 4.2. *Let $\sigma \in \{\sigma_L, \sigma_U\}$, with σ_L and σ_U as defined in Lemma 2.1, define the operator $\mathcal{L}^{1,\sigma} = -\varepsilon \frac{d^2}{dx^2} + \sigma x$, and write $\{\mu_n^{1,\sigma}\}$ for the eigenvalues corresponding to the problem*

$$(4.10) \quad \mathcal{L}^{1,\sigma} w = \mu_n^{1,\sigma} w, \quad \text{with} \quad \mathcal{G}(w, 0) = \mathcal{G}(w, 1) = 0.$$

Let $\{\mu_n^{1,\sigma}\}$ be arranged so that $\mu_0^{1,\sigma} \leq \mu_1^{1,\sigma} \leq \dots \leq \mu_n^{1,\sigma} \leq \dots$. Then,

$$(4.11) \quad \mu_n^{1,\sigma_L} \leq \mu_n \leq \mu_n^{1,\sigma_U} \quad \text{for all} \quad n \in \mathbf{N} \cup \{0\}.$$

Proof. First, we decompose \mathcal{L} as

$$(4.12) \quad \mathcal{L} = \mathcal{L}^{1,\sigma} + \mathcal{F}^{1,\sigma}, \quad \text{where} \quad \mathcal{L}^{1,\sigma} = -\varepsilon \frac{d^2}{dx^2} + \sigma x, \quad \mathcal{F}^{1,\sigma} = F(x) - \sigma x,$$

and $\sigma \in \{\sigma_L, \sigma_U\}$. We note here that $\mathcal{L}^{1,\sigma}$ is self-adjoint.

Next, \mathcal{F}^{1,σ_L} is a positive definite multiplicative operator, since $F(x) \geq \sigma_L x$ (see (2.2)). Thus, $\mu_n^{1,\sigma_L} \leq \mu_n$ for all $n \in \mathbf{N} \cup \{0\}$, by Theorem 4.1. In contrast, \mathcal{F}^{1,σ_U} is negative definite, since $F(x) \leq \sigma_U x$. Therefore, we write

$$\mathcal{L}^{1,\sigma_U} = \mathcal{L} - \mathcal{F}^{1,\sigma_U},$$

where now $-\mathcal{F}^{1,\sigma_U}$ is positive definite. The fact that the spectrum $\{\mu_n\}$ is bounded from below by Lemma 4.1 allows us to use Theorem 4.1 to bound each μ_n from above, $\mu_n \leq \mu_n^{1,\sigma_U}$. Combining both bounds for each n , we obtain (4.11). \square

Hence, it remains to solve the eigenvalue problem (4.10). Although this problem is not explicitly solvable, the eigenvalues may be calculated up to terms exponentially small in ε . Letting

$$(4.13) \quad \mu_0^{*,\sigma} = \lambda^* - \lambda_0^{*,\sigma} = -A\beta^{-2} B_{0,\sigma} \quad \text{and} \quad \mu_n^{*,\sigma} = \lambda^* - \lambda_n^{*,\sigma} = \gamma A\beta^{-2} |A'_{n,\sigma}| > 0, \\ n \in \mathbf{N},$$

where we have recalled the definitions in section 2, we can prove the following lemma.

LEMMA 4.3. *Let $M \in \mathbf{N}$ be fixed, and define*

$$\delta_{0,\sigma} = \gamma^2 \exp\left(-\frac{2}{3}\gamma^{-3/2} \left[3(1 + B_{0,\sigma} - B)^{3/2} - 2(B_{0,\sigma} - B)^{3/2} - (1 + B_{0,\sigma} + B)^{3/2}\right]\right), \\ \delta_{n,\sigma} = \sqrt{\gamma} A^{1/6} \beta^{-1/3} \exp\left(-\frac{4}{3}\gamma^{-3/2} + 2|A_{n+1}| \gamma^{-1/2}\right) \quad \text{for all} \quad 1 \leq n \leq M+1$$

and for all $0 < B < B_{0,\sigma}$ for which the exponent in the expression for $\delta_{0,\sigma}$ is negative. Then, for each such B , there exists an $\varepsilon_0 > 0$ and positive constants C_0, \dots, C_{M+1} such that, for all $0 < \varepsilon < \varepsilon_0$ and $0 \leq n \leq M$, the first $M+1$ eigenvalues $\mu_0^{1,\sigma}, \dots, \mu_M^{1,\sigma}$ corresponding to (4.10) satisfy the following:

(a) For $\beta > 1$, $|\mu_0^{1,\sigma} - \mu_0^{*,\sigma}| < C_0 \delta_{0,\sigma}$ and $|\mu_n^{1,\sigma} - \mu_n^{*,\sigma}| < C_n \delta_{n,\sigma}$ for all $1 \leq n \leq M$.

(b) For $0 < \beta < 1$, $|\mu_n^{1,\sigma} - \mu_{n+1}^{*,\sigma}| < C_{n+1} \delta_{n+1,\sigma}$ for all $0 \leq n \leq M$.

Lemmas 4.2 and 4.3 in combination with definitions (2.5) and (4.13) yield Theorem 2.1. The bounds on $\mu_0^{1,\sigma}, \dots, \mu_M^{1,\sigma}$ are derived in section 5. The fact that these are indeed the $M+1$ first eigenvalues corresponding to (4.10) is proved in section 6. Note that Theorem 2.1 follows immediately from this lemma, in combination with the above analysis and the observation that the condition $\beta > 1$ is equivalent to $0 < \sigma < A$, and the condition $0 < \beta < 1$ equivalent to $\sigma > A$.

5. The eigenvalues $\mu_0^{1,\sigma}, \dots, \mu_M^{1,\sigma}$. In this section, we derive the bounds on $\mu_0^{1,\sigma}, \dots, \mu_M^{1,\sigma}$ of Lemma 4.3. In section 5.1, we reduce the eigenvalue problem (4.10) to the algebraic one of locating the roots of an Evans-type function \mathcal{D} . In section 5.2, we identify the roots of \mathcal{D} with those of two functions \mathcal{A} and \mathcal{B} which are related to the Airy functions and simpler to analyze than \mathcal{D} . Finally, in section 5.3, we identify the relevant roots of \mathcal{A} and \mathcal{B} and thus also of \mathcal{D} .

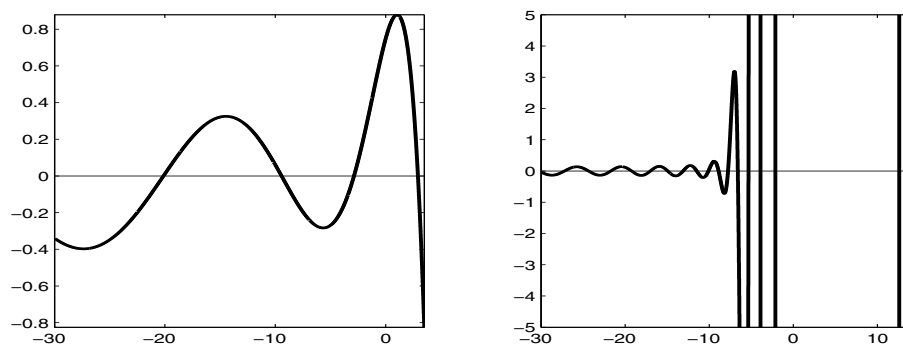


FIG. 5.1. The function $\mathcal{D}(\bar{\chi})$ for $a = 3$, $\sigma = 1$, and $\varepsilon = 0.1$ (left panel), $\varepsilon = 0.001$ (right panel).

5.1. Reformulation of the eigenvalue problem. First, we derive an algebraic equation, the solutions of which correspond to the eigenvalues of (4.10). We start by rescaling the eigenvalue $\mu^{1,\sigma}$ and the independent variable x via

$$(5.1) \quad \bar{\chi} = -\gamma^{-1} A^{-1} \beta^2 \mu^{1,\sigma} \quad \text{and} \quad x = \gamma(\chi - \bar{\chi}).$$

Then, we define the linear functional

$$(5.2) \quad \Gamma(w, \bar{\chi}) = w(\bar{\chi}) - \sqrt{\gamma} \beta^{-1} w'(\bar{\chi}) \quad \text{for all differentiable functions } w,$$

and we remark that, for w equal to Ai or Bi, this definition agrees with that given in (2.4). Further introducing the Wronskian

$$(5.3) \quad \mathcal{D}(\bar{\chi}) = \Gamma(\text{Ai}, \bar{\chi}) \Gamma(\text{Bi}, \gamma^{-1} + \bar{\chi}) - \Gamma(\text{Ai}, \gamma^{-1} + \bar{\chi}) \Gamma(\text{Bi}, \bar{\chi})$$

(see also Figure 5.1), we can prove the following lemma.

LEMMA 5.1. *The eigenvalue problem (4.10) has $\mu^{1,\sigma}$ as an eigenvalue if and only if $\mathcal{D}(\bar{\chi}) = 0$.*

Proof. Using (5.1), we rewrite problem (4.10) in the form

$$(5.4) \quad \begin{aligned} \frac{d^2 w}{d\chi^2} &= \chi w, \quad \chi \in [\bar{\chi}, \gamma^{-1} + \bar{\chi}], \\ \Gamma(w, \bar{\chi}) &= \Gamma(w, \gamma^{-1} + \bar{\chi}) = 0. \end{aligned}$$

This is an Airy equation and thus has the general solution

$$(5.5) \quad w(\chi) = D_A \text{Ai}(\chi) + D_B \text{Bi}(\chi).$$

The boundary conditions become

$$(5.6) \quad \begin{aligned} \Gamma(w, \bar{\chi}) &= D_A \Gamma(\text{Ai}, \bar{\chi}) + D_B \Gamma(\text{Bi}, \bar{\chi}) &= 0, \\ \Gamma(w, \gamma^{-1} + \bar{\chi}) &= D_A \Gamma(\text{Ai}, \gamma^{-1} + \bar{\chi}) + D_B \Gamma(\text{Bi}, \gamma^{-1} + \bar{\chi}) &= 0. \end{aligned}$$

The sufficient and necessary condition for the existence of nontrivial solutions to this system is that its determinant—which is the Wronskian \mathcal{D} given in (5.3)—vanishes, and the lemma is proved. \square

5.2. Product decomposition of the function \mathcal{D} . In the preceding section, we saw that the values of $\bar{\chi}$ corresponding to the eigenvalues $\mu^{1,\sigma}$ must be zeroes of \mathcal{D} . In the next section, we will prove that the first few zeroes of \mathcal{D} are all $\mathcal{O}(1)$, in the case $0 < \beta < 1$, and both $\mathcal{O}(1)$ and $\mathcal{O}(\gamma^{-1})$ in the case $\beta > 1$. To identify them, we rewrite \mathcal{D} in the form

$$(5.7) \quad \mathcal{D}(\bar{\chi}) = \Gamma(\text{Bi}, \gamma^{-1} + \bar{\chi}) \mathcal{A}(\bar{\chi}) = \Gamma(\text{Ai}, \bar{\chi}) \mathcal{B}(\bar{\chi}),$$

where we have defined the functions

$$(5.8) \quad \mathcal{A}(\bar{\chi}) = \Gamma(\text{Ai}, \bar{\chi}) - \frac{\Gamma(\text{Ai}, \gamma^{-1} + \bar{\chi})}{\Gamma(\text{Bi}, \gamma^{-1} + \bar{\chi})} \Gamma(\text{Bi}, \bar{\chi}),$$

$$(5.9) \quad \mathcal{B}(\bar{\chi}) = \Gamma(\text{Bi}, \gamma^{-1} + \bar{\chi}) - \frac{\Gamma(\text{Bi}, \bar{\chi})}{\Gamma(\text{Ai}, \bar{\chi})} \Gamma(\text{Ai}, \gamma^{-1} + \bar{\chi}).$$

Here, \mathcal{A} is well defined for all $\bar{\chi}$ such that $\Gamma(\text{Bi}, \gamma^{-1} + \bar{\chi}) \neq 0$, while \mathcal{B} is well defined for all $\bar{\chi}$ such that $\Gamma(\text{Ai}, \bar{\chi}) \neq 0$. Equation (5.7) implies that the roots of \mathcal{A} and \mathcal{B} are also roots of \mathcal{D} .

In the next section, we will establish that the $\mathcal{O}(1)$ roots of \mathcal{D} coincide with roots of \mathcal{A} and the $\mathcal{O}(\gamma^{-1})$ ones with roots of \mathcal{B} . To prove this, we first characterize the behaviors of \mathcal{A} and \mathcal{B} for $\mathcal{O}(1)$ and $\mathcal{O}(\gamma^{-1})$ values of $\bar{\chi}$, respectively, by means of the next two lemmas. In what follows, we write $E(x) = \exp(-(2/3)x^{3/2})$ for brevity and $\|\cdot\|_{[X_L, X_R]}$ for the W_∞^1 -norm over any interval $[X_L, X_R]$,

$$(5.10) \quad \|w\|_{[X_L, X_R]} = \max_{\bar{\chi} \in [X_L, X_R]} |w(\bar{\chi})| + \max_{\bar{\chi} \in [X_L, X_R]} |w'(\bar{\chi})|.$$

LEMMA 5.2. *Let $X < 0$ be fixed. Then there is a $\gamma_0 > 0$ and a constant $c_A > 0$ such that*

$$(5.11) \quad \|\mathcal{A}(\cdot) - \Gamma(\text{Ai}, \cdot)\|_{[X, 0]} < c_A \gamma^{-1/2} E(\gamma^{-1}(2 + 3\gamma X)^{2/3}) \quad \text{for all } 0 < \gamma < \gamma_0.$$

For the next lemma, we switch to the independent variable $\bar{\psi} = \gamma\bar{\chi}$ to facilitate calculations. We analyze the behavior of $\mathcal{B}(\gamma^{-1}\bar{\psi})$ for $\mathcal{O}(1)$ values of $\bar{\psi}$ (equivalently, for $\mathcal{O}(\gamma^{-1})$ values of $\bar{\chi}$) as $\gamma \downarrow 0$.

LEMMA 5.3. *Let $0 < \Psi_L < \Psi_R$ be fixed. Then there is a $\gamma_0 > 0$ and a constant $c_B > 0$ such that, for all $0 < \gamma < \gamma_0$,*

$$\begin{aligned} & \|E(\gamma^{-1}(1 + \bar{\psi})) [\mathcal{B}(\gamma^{-1}\bar{\psi}) - \Gamma(\text{Bi}, \gamma^{-1}(1 + \bar{\psi}))]\|_{\bar{\psi} \in [\Psi_L, \Psi_R]} \\ & < c_B \gamma^{-1/4} \left[\frac{E(\gamma^{-1}(1 + \Psi_L))}{E(\gamma^{-1}\Psi_L)} \right]^2. \end{aligned}$$

The proofs of these lemmas are given in Appendices B and C, respectively.

5.3. Zeroes of \mathcal{D} . Using Lemma 5.2 and an auxiliary result, we can locate the roots of \mathcal{D} .

LEMMA 5.4. *Let $M \in \mathbf{N}$ be fixed, $A'_{n,\sigma}$ and $B_{0,\sigma}$ be defined as in section 2, and $B, \delta_{0,\sigma}, \dots, \delta_{M,\sigma}$ be defined as in Lemma 4.3. Then, for each admissible B , there is a $\gamma_0 > 0$ and positive constants c_0, \dots, c_M such that, for all $0 < \gamma < \gamma_0$, $\mathcal{D}(\bar{\chi})$ has roots $\bar{\chi}_0 > \bar{\chi}_1 > \dots > \bar{\chi}_M$ satisfying the following bounds:*

(a) *For $\beta > 1$,*

$$|\bar{\chi}_0 - \gamma^{-1}B_{0,\sigma}| < c_0 \gamma^{-1} \delta_{0,\sigma} \quad \text{and} \quad |\bar{\chi}_n - A'_{n,\sigma}| < c_n \gamma^{-1} \delta_{n,\sigma} \quad \text{for all } 1 \leq n \leq M.$$

(b) For $0 < \beta < 1$,

$$|\bar{\chi}_n - A'_{n+1,\sigma}| < c_n \gamma^{-1} \delta_{n+1,\sigma} \quad \text{for all } 0 \leq n \leq M.$$

The proof of this lemma requires the following elementary result.

LEMMA 5.5. *Let C and G be real-valued continuous functions and H be real-valued and differentiable. Let $\delta > 0$ and $z_0 \in [Z_L, Z_R] \subset \mathbf{R}$ be such that*

$$\begin{aligned} H(z_0) = 0, \quad \max_{[Z_L, Z_R]} H' = -H_0 < 0, \quad \max_{[Z_L, Z_R]} |C(G - H)| < \delta, \\ \text{and} \quad \min_{[Z_L, Z_R]} C = C_0 > 0. \end{aligned}$$

If $\delta < C_0 H_0 \min(z_0 - Z_L, Z_R - z_0)$, then G has a zero z_ such that $|z_* - z_0| \leq \delta / (C_0 H_0)$.*

Proof. Let $z_\ell = z_0 - \delta / (C_0 H_0)$ and $z_r = z_0 + \delta / (C_0 H_0)$. Since $Z_L < z_\ell < z_0 < z_r < Z_R$, we have

$$\begin{aligned} G(z_\ell) &= H(z_\ell) + G(z_\ell) - H(z_\ell) \geq \int_{z_0}^{z_\ell} H'(z) dz - \frac{\max_{[Z_L, Z_R]} |C(G - H)|}{\min_{[Z_L, Z_R]} C} \\ &> (z_0 - z_\ell) H_0 - \frac{\delta}{C_0} = 0. \end{aligned}$$

Similarly, we may prove that $G(z_r) < 0$, and the desired result follows. \square

Proof of Lemma 5.4. (a) First, we prove the existence of a root $\bar{\chi}_0$ satisfying the desired bound. We recall that $\bar{\psi}$ was defined above via $\bar{\psi} = \gamma \bar{\chi}$; hence, it suffices to show that there is a root $\bar{\psi}_0$ of $\mathcal{D}(\gamma^{-1} \bar{\psi})$ satisfying the bound $|\bar{\psi}_0 - B_{0,\sigma}| < c_0 \delta_0$ for some $c_0 > 0$. Equation (5.7) reads $\mathcal{D}(\gamma^{-1} \bar{\psi}) = \Gamma(\text{Ai}, \gamma^{-1} \bar{\psi}) \mathcal{B}(\gamma^{-1} \bar{\psi})$. Here, $\Gamma(\text{Ai}, \gamma^{-1} \bar{\psi})$ has no positive roots, by definition of Γ and because $\text{Ai}(\gamma^{-1} \bar{\psi}) > 0$ and $\text{Ai}'(\gamma^{-1} \bar{\psi}) < 0$ for all $\bar{\psi} > 0$. Thus, $\bar{\chi}_0$ must be a root of \mathcal{B} . Its existence and the bound on it follow from Lemmas 5.3 and 5.5. Indeed, let $z_0 = B_{0,\sigma}$, $Z_L = B_{0,\sigma} - B$, $Z_R = B_{0,\sigma} + B$, $C = E$ (see section 5.2), $G = B$, and $H = \Gamma(\text{Bi}, \cdot)$. Lemma 5.3 provides a bound δ on $|C(G - H)|_{[Z_L, Z_R]}$. Also, using Corollary A.1, we may calculate

$$\begin{aligned} C_0 &= \min_{[Z_L, Z_R]} E(\gamma^{-1}(1 + \bar{\psi})) = E(\gamma^{-1}(1 + Z_R)), \\ -H_0 &= \max_{[Z_L, Z_R]} \Gamma(\text{Bi}', \gamma^{-1}(1 + \bar{\psi})) < -c \gamma^{5/4} [E(\gamma^{-1}(1 + Z_L))]^{-1}. \end{aligned}$$

Now, δ satisfies the condition $\delta < C_0 H_0 B$ of Lemma 5.5 for all γ small enough. Thus, we may apply Lemma 5.5 to obtain the desired bound on $\bar{\chi}_0$.

Next, we show that \mathcal{A} has the remaining roots $\bar{\chi}_1, \dots, \bar{\chi}_M$. We fix $A_{M+1} < X < A_M$ and let I_1, \dots, I_M be disjoint intervals around the first M zeroes of Ai , A_1, \dots, A_M , respectively. Lemma 5.2 states that $\mathcal{A}(\bar{\chi})$ and $\Gamma(\text{Ai}, \bar{\chi})$ are exponentially close in the W_∞^1 -norm over $[X, 0]$. Thus, for all $0 < \gamma < \gamma_0$ (with γ_0 small enough), \mathcal{A} has M distinct roots $\bar{\chi}_1 \in I_1, \dots, \bar{\chi}_M \in I_M$ in $[X, 0]$ by Lemma A.2. Since $\Gamma(\text{Bi}, \gamma^{-1} + \bar{\chi})$ can be bounded away from zero over $[X, 0]$ using Lemma A.1 (with $p = 1$ and $q = \bar{\chi}$), we conclude that \mathcal{D} has the M distinct roots $\bar{\chi}_1, \dots, \bar{\chi}_M$ in $[X, 0]$.

(b) The argument used in part (a)—where $\beta > 1$ —to establish the bounds on the $\mathcal{O}(1)$ roots of \mathcal{A} does not depend on the sign of $\beta - 1$. Therefore, it applies also to this case—where $0 < \beta < 1$ —albeit in an interval $[X, 0]$, with $A_{M+2} < X < A_{M+1}$, yielding $M + 1$ roots which we label $\bar{\chi}_0, \dots, \bar{\chi}_M$.

On the other hand, $B_{0,\sigma} < 0$ for $0 < \beta < 1$, because of the estimate on $B_{0,\sigma}$ in Lemma A.2. As a result, the argument used to identify that root does not apply any

more, since now $B_{0,\sigma} < 0$ and thus Lemma 5.3 may not be applied to provide the bound δ needed in Lemma 5.5. In fact, were this root to persist and remain close to $\gamma^{-1}B_{0,\sigma}$ as in case (a), it would become *large* and *negative* by the estimate in Lemma A.2 and hence smaller than the roots $\bar{\chi}_0, \dots, \bar{\chi}_M$ obtained above. Thus, it could never be the leading eigenvalue in this parameter regime. \square

6. The eigenfunctions $w_0^{1,\sigma}, \dots, w_M^{1,\sigma}$. In the previous section, we located some of the eigenvalues $\mu^{1,\sigma}$. In this section, we show that the eigenvalues we identified are the largest ones. To achieve this, we derive formulas for the eigenfunctions $w_0^{1,\sigma}, \dots, w_M^{1,\sigma}$ associated with $\mu_0^{1,\sigma}, \dots, \mu_M^{1,\sigma}$, respectively, and show that $w_n^{1,\sigma}$ has n zeroes in the interval $[\bar{\chi}_n, \gamma^{-1} + \bar{\chi}_n]$ (corresponding to the interval $[0, 1]$ in terms of x ; see (5.1)). The desired result follows, then, from standard Sturm–Liouville theory [4]. In particular, we prove the following lemma.

LEMMA 6.1. *Let $M \in \mathbf{N}$. Then, there is a $\gamma_0 > 0$ such that, for all $0 < \gamma < \gamma_0$ and for all $n = 0, 1, \dots, M$, the eigenfunction $w_n^{1,\sigma}$ corresponding to the eigenvalue $\mu_n^{1,\sigma}$ has exactly n zeroes in the interval $[\bar{\chi}_n, \gamma^{-1} + \bar{\chi}_n]$.*

The proof of this lemma occupies the rest of this section. Parallel to it, we show that the profile of ω_0 associated with w_0 through (4.1) is that of (a) a boundary layer near the bottom of the water column (BL) for $\beta > 1$, and (b) an interior, nonmonotone boundary layer (a *spike* [9]) close to the point $0 < x_{\text{DCM}} = \beta^2 < 1$ (DCM) for $0 < \beta < 1$.

We start by fixing $\bar{\chi}$ to be $\bar{\chi}_n$, for some $n = 1, \dots, M$. The corresponding eigenvalue is $\mu_n^{1,\sigma} = -\gamma\sigma\bar{\chi}_n$ (see (5.1)), while the corresponding eigenfunction w_n is given by (5.5),

$$(6.1) \quad w_n^{1,\sigma}(\chi) = D_A \text{Ai}(\chi) + D_B \text{Bi}(\chi), \quad \text{where } \chi \in [\bar{\chi}_n, \gamma^{-1} + \bar{\chi}_n].$$

Here, the coefficients D_A and D_B satisfy (5.6),

$$D_A \Gamma_{L,n}(\text{Ai}) + D_B \Gamma_{L,n}(\text{Bi}) = D_A \Gamma_{R,n}(\text{Ai}) + D_B \Gamma_{R,n}(\text{Bi}) = 0,$$

where $\Gamma_{L,n}(\cdot) = \Gamma(\cdot, \bar{\chi}_n)$ and $\Gamma_{R,n}(\cdot) = \Gamma(\cdot, \gamma^{-1} + \bar{\chi}_n)$. We treat the cases $\beta > 1$ and $0 < \beta < 1$ separately.

6.1. The case $\beta > 1$. In this section, we select D_A and D_B so that (6.1) becomes

$$(6.2) \quad w_n^{1,\sigma}(\chi) = D_n \text{Bi}(\chi) - \text{Ai}(\chi), \quad \text{with } D_n = \frac{\Gamma_{L,n}(\text{Ai})}{\Gamma_{L,n}(\text{Bi})} = \frac{\Gamma_{R,n}(\text{Ai})}{\Gamma_{R,n}(\text{Bi})}.$$

Using this formula, we prove Lemma 6.1 and verify that ω_0 is of boundary layer type near $x = 1$.

6.1.1. The eigenfunction $w_0^{1,\sigma}$. First, we show that $w_0^{1,\sigma}$ has no zeroes in the corresponding interval. Using Lemma A.1 and the estimates of Lemmas 5.4 for $\bar{\chi}_0$ and A.2 for $B_{0,\sigma}$, we estimate

$$D_0 = \left(\frac{\Delta_1^2}{2} + \bar{C}_0(\gamma) \right) \exp \left(-4 \left(\frac{(\beta^2 - 1)^{3/4}}{3\gamma^{3/2}} + \sqrt{1 - \frac{1}{\beta^2}} \right) \right).$$

Here, $\Delta_1 = \beta + \sqrt{\beta^2 - 1}$ and $|\bar{C}_0(\gamma)| < c_0\sqrt{\gamma}$, for some $c_0 > 0$. Thus also, $D_0 > 0$.

It suffices to show that $w_0^{1,\sigma}$ is positive in this interval, and thus that $(w_0^{1,\sigma})' > 0$ everywhere on the interval and $w_0^{1,\sigma}(\bar{\chi}_0) > 0$. For $n = 0$, (6.2) yields $(w_0^{1,\sigma})'(\chi) =$

$D_0 \text{Bi}'(\chi) - \text{Ai}'(\chi)$, while Lemma 5.4 shows that $[\bar{\chi}_0, \gamma^{-1} + \bar{\chi}_0] \subset \mathbf{R}_+$. Hence, $\text{Bi}'(\chi) > 0$ and $\text{Ai}'(\chi) < 0$ for all χ in this interval. Since $D_0 > 0$, we conclude that $(w_0^{1,\sigma})' > 0$, as desired. Next, we determine the sign of $w_0^{1,\sigma}(\bar{\chi}_0)$. This function is given in (6.2) with $n = 0$, while the definition of $\Gamma_{L,0}$ yields

$$\text{Ai}(\bar{\chi}_0) = \Gamma_{L,0}(\text{Ai}) + \beta^{-1} \sqrt{\gamma} \text{Ai}'(\bar{\chi}_0) \quad \text{and} \quad \text{Bi}(\bar{\chi}_0) = \Gamma_{L,0}(\text{Bi}) + \beta^{-1} \sqrt{\gamma} \text{Bi}'(\bar{\chi}_0).$$

Substituting into (6.2), we calculate $w_0^{1,\sigma}(\bar{\chi}_0) = \beta^{-1} \sqrt{\gamma} [D_0 \text{Bi}'(\bar{\chi}_0) - \text{Ai}'(\bar{\chi}_0)]$. Thus, $w_0^{1,\sigma}(\bar{\chi}_0)$ is positive by our remarks on the signs of Bi' , Ai' , and D_0 , and the proof is complete.

Next, we study the profile of the associated solution ω_0 to the original problem (1.14). Equations (4.1) and (5.1) yield

$$\omega_0(x) = \exp\left(\frac{\beta}{\gamma^{3/2}} x\right) [D_0 \text{Bi}(\gamma^{-1}x + \bar{\chi}_0) - \text{Ai}(\gamma^{-1}x + \bar{\chi}_0)], \quad x \in [0, 1].$$

Using the estimation of Lemma 5.4 for $\bar{\chi}_0$ and the estimations of Lemma A.1 for Ai and Bi , we find

$$\omega_0(x) = C_I(x) (x + \beta^2 - 1)^{-1/4} \exp\left(\frac{\beta}{\gamma^{3/2}} x\right) \sinh(\theta_1(x)), \quad x \in [0, 1],$$

where $C_I(x) = C_{I,0} + C_{I,1}(x)$, $\sup_{[0,1]} |C_{I,1}(x)| < c_I \sqrt{\gamma}$, for some $c_I > 0$, and

$$\theta_1(x) = \frac{2}{3\gamma^{3/2}} [(x + \beta^2 - 1)^{3/2} - (\beta^2 - 1)^{3/2}] + \frac{2}{\beta} [(x + \beta^2 - 1)^{1/2} - (\beta^2 - 1)^{1/2}] + \log \Delta_1.$$

The first two terms on the right-hand side of the expression for ω_0 are bounded, while the other two correspond to localized concentrations (boundary layers) at $x = 1$. Thus, ω_0 also corresponds to a boundary layer of width $\mathcal{O}(\gamma^{3/2}) = \mathcal{O}(\sqrt{\varepsilon})$ at the same point.

6.1.2. The eigenfunctions $w_1^{1,\sigma}, \dots, w_M^{1,\sigma}$. Next, we show that the eigenfunction $w_n^{1,\sigma}$ has n zeroes in $[\bar{\chi}_n, \gamma^{-1} + \bar{\chi}_n]$, where $n = 1, \dots, M$. The eigenfunction $w_n^{1,\sigma}$ is given by (6.2). Here also, Lemmas A.1 and 5.4 yield

$$(6.3) \quad D_n = \left(\frac{\Delta_2^2}{2} + \bar{C}_n(\gamma)\right) \exp\left(-\frac{4}{3\gamma^{3/2}} + 2\frac{|A_n|}{\sqrt{\gamma}} - \frac{2}{\beta}\right),$$

where $\Delta_2 = (\beta + 1)^{1/2} (\beta - 1)^{-1/2}$ and $|\bar{C}_n(\gamma)| < c_n \sqrt{\gamma}$, for some $c_n > 0$. Hence, $D_n > 0$.

First, we show that the function $w_n^{1,\sigma}$ has exactly $n - 1$ zeroes in $[\bar{\chi}_n, 0]$. The estimate (6.3) and the fact that Bi is uniformly bounded on $[\bar{\chi}_n, 0]$ imply that, for all $0 < \gamma < \gamma_0$ (with γ_0 small enough), the functions $w_n^{1,\sigma}$ and $-\text{Ai}$ are exponentially close in the W_∞^1 -norm over that interval,

$$(6.4) \quad \|w_n^{1,\sigma} + \text{Ai}\|_{[\bar{\chi}_n, 0]} < c_n \exp\left(-\frac{4}{3\gamma^{3/2}} + 2\frac{|A_n|}{\sqrt{\gamma}}\right) \quad \text{for some } c_n > 0.$$

As a result, we may use an argument exactly analogous to the one used in the proof of Lemma 5.4 to show that $w_n^{1,\sigma}$ has at least $n - 1$ distinct zeroes in $[\bar{\chi}_n, 0]$, each of which is exponentially close to one of A_1, \dots, A_{n-1} . Observing that $\bar{\chi}_n$ is algebraically

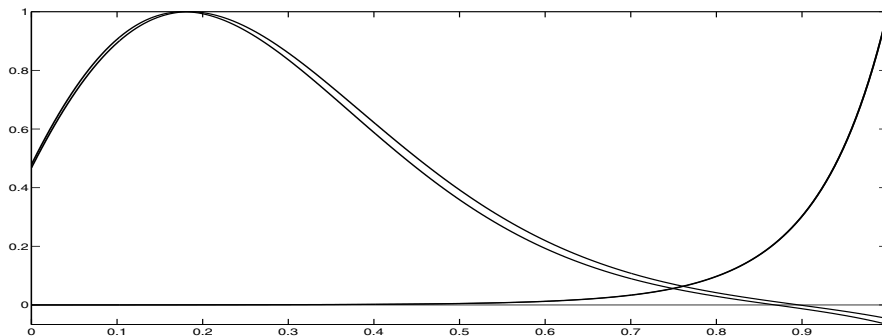


FIG. 6.1. The eigenfunctions $w_0^{1,\sigma_L}, w_0^{1,\sigma_U}$ (always positive and coinciding within plotting accuracy) and $w_1^{1,\sigma_L}, w_1^{1,\sigma_U}$ (changing sign). Here, $a = 0.775$, $n_H = 0.667$, $\varepsilon = 0.001$, $\kappa = 1$, $\ell = 0.25$, and $j_H = 0.5$, which yields $\sigma_L = 0.1333$, $\sigma_U = 0.1457$ (and thus $\sigma_L < \sigma_U < a^2/4$), $0.0104 \leq \lambda_0 \leq 0.0222$, and $-0.0541 \leq \lambda_1 \leq -0.0512$. Note that $\lambda_1 < \lambda_0$ and that none of w_0^{1,σ_L} and w_0^{1,σ_U} has zeroes in $[0, 1]$, while w_1^{1,σ_L} and w_1^{1,σ_U} have exactly one zero in the same interval.

larger than A_n , by Lemmas 5.4 and A.2, while $w_n^{1,\sigma}$ is exponentially close to $-\text{Ai}$, by estimate (6.4), we conclude that the zero of $w_n^{1,\sigma}$ close to A_n lies to the left of $\bar{\chi}_n$ (and hence outside $[\bar{\chi}_n, 0]$) and thus there are no other zeroes in $[\bar{\chi}_n, \gamma^{-1} + \bar{\chi}_n]$.

It remains to show only that there is a unique zero of $w_n^{1,\sigma}$ in $[0, \gamma^{-1} + \bar{\chi}_n]$. We work as in section 6.1.1 and show that $w_n^{1,\sigma}$ is increasing and changes sign in that interval. First, we calculate $(w_n^{1,\sigma})'(\chi) = D_n \text{Bi}'(\chi) - \text{Ai}'(\chi) > 0$, where we have used that $\text{Bi}'(\chi) > 0$, $\text{Ai}'(\chi) < 0$, and $D_n > 0$. Also, $w_n^{1,\sigma}(0) < 0$ (by $\text{Ai}(0) > 0$ and (6.4)) and, working as in section 6.1.1,

$$w_n^{1,\sigma}(\gamma^{-1} + \bar{\chi}_n) = \beta^{-1} \sqrt{\gamma} [D_n \text{Bi}'(\gamma^{-1} + \bar{\chi}_n) - \text{Ai}'(\gamma^{-1} + \bar{\chi}_n)] > 0.$$

This completes the proof.

6.2. The case $0 < \beta < 1$. In this section, we select D_A and D_B so that (6.1) becomes

$$(6.5) \quad w_n^{1,\sigma}(\chi) = \text{Ai}(\chi) + D_n \text{Bi}(\chi), \quad \text{with } D_n = -\frac{\Gamma_{L,n}(\text{Ai})}{\Gamma_{L,n}(\text{Bi})} = -\frac{\Gamma_{R,n}(\text{Ai})}{\Gamma_{R,n}(\text{Bi})}.$$

Using this formula, we prove Lemma 6.1 and verify that the profile of ω_0 has a spike around $x_\beta = \beta^2$.

We shall show that the eigenfunction $w_n^{1,\sigma}$ ($n = 0, \dots, M$) has n zeroes in $[\bar{\chi}_n, \gamma^{-1} + \bar{\chi}_n]$; see Figure 6.1. The proof is entirely analogous to that in section 6.1.2. Here also, the n th eigenvalue is $\mu_n^{1,\sigma} = -\gamma\sigma\bar{\chi}_n$, while the corresponding eigenfunction $w_n^{1,\sigma}$ is given by (6.5). The constant D_n may be estimated by

$$(6.6) \quad D_n = \left(\frac{\Delta_3^2}{2} + \hat{C}_n(\gamma) \right) \exp \left(-\frac{4}{3\gamma^{3/2}} + 2\frac{|A_{n+1}|}{\sqrt{\gamma}} - \frac{2}{\beta} \right),$$

where $\Delta_3 = \sqrt{1+\beta}/\sqrt{1-\beta}$ and $|\hat{C}_n| < c'_n \sqrt{\gamma}$ for some $c'_n > 0$. This is an estimate of the same type as (6.3) but with A_{n+1} replacing A_n . Thus, the estimate (6.4) holds here as well with the same change. Recalling that $\bar{\chi}_n$ is algebraically larger than

A_{n+1} (see Lemmas 5.4 and A.2), we conclude that $w_n^{1,\sigma}$ has n distinct zeroes, each of which is exponentially close to one of A_1, \dots, A_n . Next, we show that $w_n^{1,\sigma} > 0$ in $[0, \gamma^{-1} + \bar{\chi}_n]$ and thus has no extra zeroes. First, $w_n^{1,\sigma}(\chi) = \text{Ai}(\chi) + D_n \text{Bi}(\chi)$. Now, $\text{Bi}(\chi) > 0$ and $\text{Ai}(\chi) > 0$, for all $\chi \in [0, \gamma^{-1} + \bar{\chi}_n]$, while $D_n > 0$ by (6.6). Hence, $w_n^{1,\sigma} > 0$, and the proof is complete.

Next, we examine the solution ω_0 associated with w_0 . Working as in section 6.1.1, we calculate

$$\omega_0(x) = C_{II}(x)x^{-1/4} \exp\left(\frac{\beta}{\gamma^{3/2}}x\right) \cosh(\theta_2(x)), \quad x \in [0, 1],$$

where $C_{II}(x) = C_{II,0} + C_{II,1}(x)$, $\sup_{[0,1]} |C_{II,1}(x)| < c_{II} \sqrt{\gamma}$ for some $c_{II} > 0$, and

$$\theta_2(x) = \frac{2}{3\gamma^{3/2}}(1 - x^{3/2}) - \left(\frac{|A_1|}{\sqrt{\gamma}} - \frac{1}{\beta}\right)(1 - \sqrt{x}) - \log \Delta_3.$$

The first two terms on the right-hand side of the expression for ω_0 are bounded, while the other two correspond to boundary layers at $x = 1$ and $x = 0$, respectively. A straightforward calculation shows that ω_0 corresponds to a spike of width $\mathcal{O}(\gamma^{3/4}) = \mathcal{O}(\varepsilon^{1/4})$ around the point x_β , where

$$(6.7) \quad |x_\beta - (\beta^2 + |A_1|\gamma)| < c\gamma^2 \quad \text{for some } c > 0.$$

We remark that x_β does *not* correspond to the position of the DCM for the problem (1.14) involving the function f . This information is obtained in the next section, instead, through a WKB analysis.

7. The WKB approximation. In the previous sections, we derived strict bounds for the eigenvalues μ_1, \dots, μ_M of \mathcal{L} and summarized them in Theorem 2.1. In this section, we use the WKB method to derive explicit (albeit asymptotic) formulas for these eigenvalues. The outcome of this analysis has already been summarized in section 2.1.

7.1. The case $A < \sigma_L$.

7.1.1. WKB formulas for w . The eigenvalue problem (4.2) reads

$$(7.1) \quad \varepsilon w_{xx} = (F(x) - \mu)w, \quad \text{with } \mathcal{G}(w, 0) = \mathcal{G}(w, 1) = 0.$$

Since we are interested in the regime $\sigma_L > A$, Lemma 4.3 states that the eigenvalues μ_0, \dots, μ_M lie in a $\mathcal{O}(\varepsilon^{1/3})$ region to the right of zero. Thus, for any $0 \leq n \leq M$,

$$F(x) < \mu_n \quad \text{for } x \in [0, \bar{x}_n], \quad \text{and} \quad F(x) > \mu_n \quad \text{for } x \in (\bar{x}_n, 1].$$

Here, \bar{x}_n corresponds to a *turning point*, i.e., $F(\bar{x}_n) = \mu_n$, and it is given by the formula

$$(7.2) \quad \bar{x}_n = \frac{1}{\kappa} \log \frac{1 + \mu_n(1 + \eta_H)(1 + j_H^{-1})}{1 - \mu_n(1 + \eta_H)(1 + j_H)}.$$

Lemmas 4.3 and A.2 suggest that the eigenvalue μ_n may be expanded asymptotically in powers of $\varepsilon^{1/6}$ starting with $\mathcal{O}(\varepsilon^{1/3})$ terms, $\mu_n = \sum_{\ell=2}^{\infty} \varepsilon^{\ell/6} \mu_{n,\ell}$. Thus, we also find

$$(7.3) \quad \bar{x}_n = \varepsilon^{1/3} \sigma_0^{-1} \mu_{n,2} + \varepsilon^{1/2} \sigma_0^{-1} \mu_{n,3} + \mathcal{O}\left(\varepsilon^{2/3}\right), \quad \text{where } \sigma_0 = F'(0).$$

The solution in the region $(\bar{x}_n, 1]$, where $F(x) - \mu_n > 0$, can be determined using standard formulas (see [2, section 10.1]),

$$(7.4) \quad w_n(x) = [F(x) - \mu_n]^{-1/4} \left[C_a \exp^{-\int_{\bar{x}_n}^x \sqrt{(F(s) - \mu_n)/\varepsilon} ds} + C_b e^{\int_{\bar{x}_n}^x \sqrt{(F(s) - \mu_n)/\varepsilon} ds} \right].$$

Here, C_a and C_b are arbitrary constants, to leading order in ε . (Higher order terms in the asymptotic expansions of C_a and C_b generally depend on x ; see [2] for details.) Using this information and the asymptotic expansion for μ_n , we may determine the principal part of the solution w_n ,

$$(7.5) \quad w_{n,0}(x) = [F(x)]^{-1/4} \left[C_{a,0} e^{-\theta_3(x)} + C_{b,0} e^{\theta_3(x)} \right],$$

for arbitrary constants $C_{a,0}$ and $C_{b,0}$ and where

$$(7.6) \quad \theta_3(x) = \frac{1}{\varepsilon^{1/2}} \int_0^x \sqrt{F(s)} ds - \frac{1}{\varepsilon^{1/6}} \frac{\mu_{n,2}}{2} \int_0^x \frac{ds}{\sqrt{F(s)}} + \frac{\mu_{n,2}}{\sqrt{\sigma_0}} - \frac{2}{3} \sqrt{\sigma_0} - \frac{\mu_{n,3}}{2} \int_0^x \frac{ds}{\sqrt{F(s)}}.$$

To determine the solution in $[0, \bar{x}_n)$, we change the independent variable through

$$(7.7) \quad x = \varepsilon^{1/3} \sigma_0^{-1/3} (\chi - \bar{\chi}_n), \quad \text{where} \quad \bar{\chi}_n = -\sigma_0^{1/3} \varepsilon^{-1/3} \bar{x}_n = -\sigma_0^{-2/3} \mu_{n,2} + \mathcal{O}(\sqrt{\varepsilon}) < 0,$$

and expand $F(x) - \mu_n = F(x) - F(\bar{x}_n)$ asymptotically:

$$(7.8) \quad F(x) - F(\bar{x}_n) = F(\varepsilon^{1/3} \sigma_0^{-1/3} (\chi - \bar{\chi}_n)) - F(-\varepsilon^{1/3} \sigma_0^{-1/3} \bar{\chi}_n) = \varepsilon^{1/3} \sigma_0^{2/3} \chi + \mathcal{O}(\sqrt{\varepsilon}).$$

As a result, (7.1) becomes the Airy equation $(w_n)_{\chi\chi} = \chi w_n$, to leading order, whence

$$(7.9) \quad w_{n,0}(\chi) = D_{a,0} \text{Ai}(\chi) + D_{b,0} \text{Bi}(\chi), \quad \text{with } \chi \in (-\sigma_0^{-2/3} \mu_{n,2}, 0].$$

7.1.2. Boundary conditions for the WKB solution. Next, we determine the coefficients appearing in (7.5) and (7.9). Formula (7.5) represents the solution in the region $(\bar{x}_n, 1]$, and thus it must satisfy the boundary condition $\mathcal{G}(w_n, 1) = 0$. Using (4.3), we find, to leading order,

$$(7.10) \quad C_{a,0} (a + 2\sqrt{\sigma_1}) e^{-\theta_3(x)} + C_{b,0} (a - 2\sqrt{\sigma_1}) e^{\theta_3(x)} = 0, \quad \text{where } \sigma_1 = F(1).$$

Next, the formula given in (7.9) is valid for $\chi \in (-\sigma_0^{-2/3} \mu_{n,2}, 0]$ (equivalently, for $x \in [0, \bar{x}_n)$), and thus it must satisfy the boundary condition $\mathcal{G}(w, 0) = 0$. Recasting the formula for \mathcal{G} given in (4.3) in terms of χ , we obtain to leading order the equation

$$(7.11) \quad D_{a,0} \text{Ai}\left(-\sigma_0^{-2/3} \mu_{n,2}\right) + D_{b,0} \text{Bi}\left(-\sigma_0^{-2/3} \mu_{n,2}\right) = 0.$$

Finally, (7.5) and (7.9) must also match in an intermediate length scale to the right of $x = \bar{x}_n$ (equivalently, of $\chi = 0$). To this end, we set $\psi = \varepsilon^d (x - \bar{x}_n)$, where $1/5 < d < 1/3$ [2, section 10.4], and recast (7.5) in terms of ψ . We find, to leading order and for all $\mathcal{O}(1)$ and positive values of ψ ,

$$w_{n,0}(x(\psi)) = \varepsilon^{-d/4} \sigma_0^{-1/4} \psi^{-1/4} \left[C_{a,0} e^{-\theta_4(\psi) - \sigma_0^{-1} (\mu_{n,2})^{3/2}} + C_{b,0} e^{\theta_4(\psi) + \sigma_0^{-1} (\mu_{n,2})^{3/2}} \right],$$

where $\theta_4(\psi) = (2/3) \varepsilon^{(3d-1)/2} \sqrt{\sigma_0} \psi^{3/2}$. Similarly, (7.9) yields

$$w_{n,0}(\chi(\psi)) = \varepsilon^{1/12-d/4} \sigma_0^{-1/12} \pi^{-1/2} \psi^{-1/4} \left[\frac{D_{a,0}}{2} e^{-\theta_4(\psi)} + D_{b,0} e^{\theta_4(\psi)} \right].$$

The matching condition around the turning point then gives

$$(7.12) \quad C_{a,0} = \varepsilon^{1/12} \frac{\sigma_0^{1/6}}{2\sqrt{\pi}} e^{\sigma_0^{-1}(\mu_{n,2})^{3/2}} D_{a,0} \quad \text{and} \quad C_{b,0} = \varepsilon^{1/12} \frac{\sigma_0^{1/6}}{\sqrt{\pi}} e^{-\sigma_0^{-1}(\mu_{n,2})^{3/2}} D_{b,0}.$$

7.1.3. The eigenvalues μ_0, \dots, μ_n . The linear system (7.10)–(7.12) has a nontrivial solution if and only if the determinant corresponding to it vanishes identically:

$$\begin{aligned} & 2(a - 2\sqrt{\sigma_1}) e^{\theta_3(1) - \sigma_0^{-1}(\mu_{n,2})^{3/2}} \text{Ai}(\sigma^{-2/3} \mu_{n,2}) \\ & + (a + 2\sqrt{\sigma_1}) e^{-\theta_3(1) + \sigma_0^{-1}(\mu_{n,2})^{3/2}} \text{Bi}(\sigma^{-2/3} \mu_{n,2}) = 0. \end{aligned}$$

Since $\sigma_1 \geq \sigma_L$ by Lemma 2.1 and $\sigma_L > A$ by assumption, $a - 2\sqrt{\sigma_1}$ is $\mathcal{O}(1)$ and negative. Also, $\theta_3(1)$ is $\mathcal{O}(1)$ and positive by (7.6). Thus, the determinant condition reduces to $\text{Ai}(\sigma^{-2/3} \mu_{n,2}) = 0$, whence $\mu_{n,2} = -\sigma_0^{2/3} A_{n+1} = \sigma_0^{2/3} |A_{n+1}| > 0$. Hence, we find for the eigenvalues of (1.14)

$$(7.13) \quad \lambda_n = \lambda^* - \varepsilon^{1/3} \sigma_0^{2/3} |A_{n+1}| + \mathcal{O}(\sqrt{\varepsilon}).$$

Working in a similar way, we find $\mu_{n,3} = -2\sigma_0/a$.

Recalling that $\sigma_0 = F'(0) = -f'(0)$ by (2.1) and Lemma 2.1 (see also Figure 2.3), we find that the WKB formula (7.13) coincides—up to and including terms of $\mathcal{O}(1)$ and $\mathcal{O}(\varepsilon^{1/3})$ —(a) for $0 < j_H < j_H^{(2)}$, with the rigorous lower bound for λ_n derived in Theorem 2.1, and (b) for $j_H > 1$, with the rigorous upper bound for λ_n derived in the same theorem. For the remaining values of j_H , (7.13) yields a value for λ_n which lies in between the upper and lower bounds derived in Theorem 2.1—indeed, in that case, $\sigma_L < F'(0) < \sigma_U$; see Figure 2.3.

7.1.4. The eigenfunctions w_0, \dots, w_n . Finally, one may determine the constants C_a , C_b , D_a , and D_b corresponding to the eigenfunction w_n , and thus also w_n itself, through (7.10)–(7.12). The principal part of w_n is given by the formula

$$(7.14) \quad w_{n,0}(x) = \begin{cases} \text{Ai}\left(A_{n+1} + \varepsilon^{-1/3} \sigma_0^{1/3} x\right) & \text{for } x \in [0, \varepsilon^{1/3} \sigma_0^{-1/3} |A_{n+1}|), \\ C[F(x)]^{-1/4} \cosh \Theta(x) & \text{for } x \in (\varepsilon^{1/3} \sigma_0^{-1/3} |A_{n+1}|, 1]. \end{cases}$$

Here,

$$(7.15) \quad C = \varepsilon^{1/12} \frac{\sigma_0^{1/6}}{2\sqrt{\pi}} \Delta_4 e^{|A_{n+1}|^{3/2} - \Theta_3(1)}, \quad \text{where } \Delta_4 = \left(\frac{\sqrt{\sigma_1} + \sqrt{A}}{\sqrt{\sigma_1} - \sqrt{A}} \right)^{1/2},$$

$$(7.16)$$

$$\Theta(x) = \varepsilon^{-1/2} \int_x^1 \sqrt{F(s)} ds - \left(\varepsilon^{-1/6} \frac{\sigma_0^{2/3} |A_{n+1}|}{2} - \frac{\sigma_0}{a} \right) \int_x^1 \frac{ds}{\sqrt{F(s)}} + \log \Delta_4.$$

Recalling (4.1), we find

$$(7.17)$$

$$\omega_{n,0}(x) = \begin{cases} e^{\sqrt{A/\varepsilon}} \text{Ai}\left(A_{n+1} + \varepsilon^{-1/3} \sigma_0^{1/3} x\right) & \text{for } x \in [0, \varepsilon^{1/3} \sigma_0^{-1/3} |A_{n+1}|), \\ C[F(x)]^{-1/4} e^{\sqrt{A/\varepsilon}} \cosh \Theta(x) & \text{for } x \in (\varepsilon^{1/3} \sigma_0^{-1/3} |A_{n+1}|, 1]. \end{cases}$$

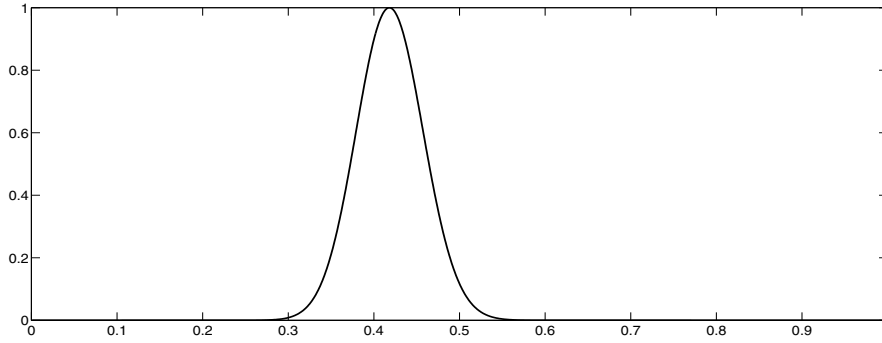


FIG. 7.1. The eigenfunction ω_0 as given by (7.17). Here, $a = 0.5$, $n_H = 0.667$, $\varepsilon = 2 \cdot 10^{-7}$, $\kappa = 1$, and $j_H = 0.5$. The eigenfunction has been scaled so that its maximum value is equal to one.

A straightforward calculation shows that ω_0 corresponds to a spike around the point

$$(7.18) \quad x_{\text{DCM}} = x_{\text{DCM},0} + \mathcal{O}(\varepsilon^{1/3}),$$

where $x_{\text{DCM},0}$ is the unique solution to $F(x_{\text{DCM},0}) = A = a^2/4$; see also Figure 7.1, where ω_0 is plotted for specific parameter values. Thus, $\omega_{0,0}$ indeed corresponds to a DCM. Furthermore, the location of the maximum phytoplankton concentration is expressed explicitly by this equation in terms of the rescaled biological parameters κ , η_H , j_H , and a .

7.2. The case $A > \sigma_U$. To obtain the eigenvalues and their corresponding eigenfunctions in this case, we work as in the preceding section. Here also, the eigenvalue problem (4.2) has the form (7.1). Since $A > \sigma_U$, the eigenvalue μ_0 is $\mathcal{O}(1)$ and negative, while μ_1, \dots, μ_M are $\mathcal{O}(\varepsilon^{1/3})$ and positive; see Lemma 4.3. Due to the qualitative difference between μ_0 and the eigenvalues of higher order, we consider them separately.

We start with the case $1 \leq n \leq M$. Then, for each such n , the eigenvalue problem (7.1) has a unique turning point \bar{x}_n given by (7.2), and the analysis presented in the preceding section applies here also. The formulas for μ_n and ω_n , $1 \leq n \leq M$, are identical to those of the preceding section, with the sole modification that A_n in (7.13)–(7.16) must be replaced by A_{n-1} . This completes the analysis for the case $1 \leq n \leq M$.

Next, we treat the case $n = 0$. Since $\mu_0 < 0 < F(x)$ for all $x \in [0, 1]$, the eigenvalue problem (7.1) corresponding to μ_0 has no turning points. Thus, the WKB formula (7.4), with $n = 0$ and \bar{x}_n replaced by zero, is valid for all $x \in [0, 1]$. Lemmas 4.3 and A.2 suggest that μ_0 may be expanded asymptotically as $\mu_0 = \sum_{\ell=0}^{\infty} \varepsilon^{\ell/2} \mu_{0,\ell}$. Using this expansion, we calculate the principal part of w_0 ,

$$(7.19) \quad w_{0,0}(x) = [F(x) - \mu_{0,0}]^{-1/4} \left[C_{a,0} e^{-\theta_5(x)} + C_{b,0} e^{\theta_5(x)} \right],$$

where $C_{a,0}$ and $C_{b,0}$ are arbitrary constants and

$$(7.20) \quad \theta_5(x) = \frac{1}{\varepsilon^{1/2}} \int_0^x \sqrt{F(s) - \mu_{0,0}} ds - \frac{\mu_{0,1}}{2} \int_0^x \frac{ds}{\sqrt{F(s) - \mu_{0,0}}}.$$

Next, recalling the boundary conditions $\mathcal{G}(w, 0) = \mathcal{G}(w, 1) = 0$, we obtain, to leading order,

$$(7.21) \quad \begin{aligned} C_{a,0}(a + 2\sqrt{-\mu_{0,0}}) + C_{b,0}(a - 2\sqrt{-\mu_{0,0}}) &= 0, \\ C_{a,0}(a + 2\sqrt{\sigma_1 - \mu_{0,0}})e^{-\theta_5(1)} + C_{b,0}(a - 2\sqrt{\sigma_1 - \mu_{0,0}})e^{\theta_5(1)} &= 0, \end{aligned}$$

where we recall that $\sigma_1 = F(1)$. Here, $\theta_5(1)$ is $\mathcal{O}(1)$ and positive by (7.20), while $a + 2\sqrt{-\mu_{0,0}} > 0$. Thus, we obtain $\mu_{0,0} = F(1) - A$, to leading order, whence

$$\lambda_{0,0} = f(1) - \ell.$$

This is precisely (2.8). Using this formula, one may also determine $C_{a,0}$ and $C_{b,0}$ to obtain $w_{0,0}$,

$$(7.22) \quad w_{0,0}(x) = [F(x) - \mu_{0,0}]^{-1/4} \sinh \Phi(x),$$

for $x \in [0, 1]$ and up to a multiplicative constant. Here,

$$\Phi(x) = \frac{1}{\varepsilon^{1/2}} \int_0^x \sqrt{F(s) - \mu_{0,0}} ds - \frac{\mu_{0,1}}{2} \int_0^x \frac{ds}{\sqrt{F(s) - \mu_{0,0}}} + \log \Delta_5,$$

where

$$\Delta_5 = \beta_1 + \sqrt{\beta_1^2 - 1} \quad \text{and} \quad \beta_1 = \frac{\sqrt{A}}{F(1)}.$$

Recalling (4.1), we find

$$\omega_{0,0}(x) = [F(x) - \mu_{0,0}]^{-1/4} e^{ax/2\sqrt{\varepsilon}} \sinh \Phi(x) \quad \text{for } x \in [0, 1].$$

The profile of ω_0 corresponds to a boundary layer at the point $x = 1$.

7.3. The transitional regime $\sigma_L < A < \sigma_U$. Equations (2.9) and (2.8) may be used to derive information for the transitional regime $\sigma_L < A < \sigma_U$ (see Theorem 2.1 and the discussion in section 2). In particular, the transition between the case where λ_0 is associated with a boundary layer (in biological terms, with a BL) and the case where it is associated with a spike (that is, with a DCM) occurs, to leading order, when $f(1) - \ell = \lambda^*$. Recalling (2.5), we rewrite this equation as

$$(7.23) \quad F(1) = f(0) - f(1) = A.$$

This condition reduces, to leading order, to $A = \sigma_U$ for $0 < j_H \leq j_H^{(1)}$, and to $A = \sigma_L$ for $j_H \geq j_H^{(2)}$. For $j_H^{(1)} < j_H < j_H^{(2)}$, this transitional value of A lies between σ_U and σ_L ; see section 2 and Figure 2.3.

Appendix A. Basic properties of the Airy functions. In this section, we summarize some properties of the Airy functions Ai and Bi which we use repeatedly.

LEMMA A.1. *Let $p > 0$ and q be real numbers. Then,*

$$\begin{aligned} \Gamma(\text{Ai}, \gamma^{-1}p + q) &= (\pi^{-1/2}/2) (\gamma p^{-1})^{1/4} \exp\left(- (2/3) (\gamma^{-1}p)^{3/2} - q (\gamma^{-1}p)^{1/2}\right) \\ &\quad \cdot \left[(1 + \beta^{-1}\sqrt{p}) \left(1 - (q^2/4) (\gamma p^{-1})^{1/2} + (q/4) (q^3/8 - 1) \gamma p^{-1}\right) \right. \\ &\quad \left. - (1/48) (5 - 5q^3 + q^6/8 - (43 - q^3 - q^6/8) \beta^{-1}\sqrt{p}) (\gamma p^{-1})^{3/2} \right], \quad \gamma \downarrow 0, \end{aligned}$$

$$\begin{aligned}
& \Gamma(\text{Bi}, \gamma^{-1}p + q) \\
&= \pi^{-1/2} (\gamma p^{-1})^{1/4} \exp\left((2/3)(\gamma^{-1}p)^{3/2} + q(\gamma^{-1}p)^{1/2}\right) \\
&\quad \cdot \left[(1 - \beta^{-1}\sqrt{p}) \left(1 + (q^2/4)(\gamma p^{-1})^{1/2} + (q/4)(q^3/8 - 1)\gamma p^{-1}\right) \right. \\
&\quad \left. + (1/48)(5 - 5q^3 + q^6/8 + (43 - q^3 - q^6/8)\beta^{-1}\sqrt{p})(\gamma p^{-1})^{3/2} \right], \quad \gamma \downarrow 0,
\end{aligned}$$

where the remainders of $\mathcal{O}(\gamma^2)$ were omitted from within the square brackets.

Proof. We derive only the first of these asymptotic expansions. The second one is derived in an entirely analogous manner. Definition (5.2) yields

$$\Gamma(\text{Ai}, \gamma^{-1}p + q) = \text{Ai}(\gamma^{-1}p + q) - \sqrt{\gamma}\beta^{-1}\text{Ai}'(\gamma^{-1}p + q).$$

Then, we recall the standard asymptotic expansions [2]

$$\begin{aligned}
\text{Ai}(z) &= \left(\pi^{-1/2} z^{-1/4}/2\right) \exp\left(-(2/3)z^{3/2}\right) \left[1 - (5/48)z^{-3/2} + \mathcal{O}(z^{-3})\right], \quad z \uparrow \infty, \\
\text{Ai}'(z) &= -\left(\pi^{-1/2} z^{1/4}/2\right) \exp\left(-(2/3)z^{3/2}\right) \left[1 + (7/48)z^{-3/2} + \mathcal{O}(z^{-3})\right], \quad z \uparrow \infty, \\
(\gamma^{-1}p + q)^r &= p^r \gamma^{-r} + \sum_{k=1}^{\infty} \frac{1}{k!} \left(\prod_{j=0}^{k-1} (r-j)\right) p^{r-k} q^k \gamma^{k-r}.
\end{aligned}$$

The desired equation now follows by combining these asymptotic expansions. \square

COROLLARY A.1. *Let p and q be as in Lemma A.1. Then, for $\gamma \downarrow 0$,*

$$\begin{aligned}
\Gamma(\text{Ai}', \gamma^{-1}p + q) &= -\left(\pi^{-1/2}/2\right) (\gamma^{-1}p)^{1/4} \exp\left(-(2/3)(\gamma^{-1}p)^{3/2} - q(\gamma^{-1}p)^{1/2}\right) \\
&\quad \cdot \left[(1 + \beta^{-1}\sqrt{p}) \left(1 - (q^2/4)(\gamma p^{-1})^{1/2}\right) \right. \\
&\quad + (q/4)((q^3/8 - 1) + (q^3/8 + 3)\beta^{-1}\sqrt{p})\gamma p^{-1} \\
&\quad \left. - (1/48)(-19 + q^3 + q^6/8 + (-7 + 7q^3 + q^6/8)\beta^{-1}\sqrt{p})(\gamma p^{-1})^{3/2} \right], \\
\Gamma(\text{Bi}', \gamma^{-1}p + q) &= \pi^{-1/2} (\gamma^{-1}p)^{1/4} \exp\left((2/3)(\gamma^{-1}p)^{3/2} + q(\gamma^{-1}p)^{1/2}\right) \\
&\quad \cdot \left[(1 - \beta^{-1}\sqrt{p}) \left(1 + (q^2/4)(\gamma p^{-1})^{1/2}\right) \right. \\
&\quad + (q/4)((q^3/8 - 1) - (q^3/8 + 3)\beta^{-1}\sqrt{p})\gamma p^{-1} \\
&\quad \left. + (1/48)(-19 + q^3 + q^6/8 - (-7 + 7q^3 + q^6/8)\beta^{-1}\sqrt{p})(\gamma p^{-1})^{3/2} \right],
\end{aligned}$$

where the remainders of $\mathcal{O}(\gamma^2)$ were omitted from within the square brackets.

Proof. Definition (5.2) and the identities $\text{Ai}''(z) = z\text{Ai}(z)$ and $\text{Bi}''(z) = z\text{Bi}(z)$ yield

$$\begin{aligned}
\Gamma(\text{Ai}', \gamma^{-1}p + q) &= \text{Ai}'(\gamma^{-1}p + q) - \sqrt{\gamma}\beta^{-1}(\gamma^{-1}p + q)\text{Ai}(\gamma^{-1}p + q), \\
\Gamma(\text{Bi}', \gamma^{-1}p + q) &= \text{Bi}'(\gamma^{-1}p + q) - \sqrt{\gamma}\beta^{-1}(\gamma^{-1}p + q)\text{Bi}(\gamma^{-1}p + q).
\end{aligned}$$

The desired result now follows from Lemma A.1. \square

LEMMA A.2. *The function $\Gamma(\text{Ai}, \bar{\chi})$ has no positive roots. Further, for any $M \in \mathbf{N}$, there is an $\varepsilon_0 > 0$ such that, for all $0 < \varepsilon < \varepsilon_0$, $\Gamma(\text{Ai}, \bar{\chi})$ has roots $A'_{M,\sigma} < \dots < A'_{1,\sigma} < 0$ satisfying*

$$|A'_{n,\sigma} - (A_n + \sqrt{\gamma}\beta^{-1})| < c_a \gamma \quad \text{for some } c_a > 0.$$

Here, $A_n < 0$ is the n th root of Ai (see Figure 2.1), and β, γ are given in (2.3). For $\beta > 1$ (equivalently, for $0 < \sigma < a^2/4$), the function $\Gamma(\text{Bi}, \gamma^{-1}(1 + \bar{\psi}))$ defined in (2.4) has a root $B_{0,\sigma} > 0$ satisfying

$$\left| B_{0,\sigma} - \left(\beta^2 - 1 + 2\gamma^{3/2}\beta^{-1} \right) \right| < c_b \gamma^3 \quad \text{for some } c_b > 0.$$

Proof. The fact that there exist no positive roots of $\Gamma(\text{Ai}, \bar{\chi})$ is immediate by the definition of $\Gamma(\text{Ai}, \bar{\chi})$ (see (2.4)) and the fact that $\text{Ai}(\bar{\chi}) > 0$ and $\text{Ai}'(\bar{\chi}) < 0$ for all $\bar{\chi} > 0$.

Next, the existence of M discrete and negative roots may be proved as follows. Fix $|A_M| < X < |A_{M+1}|$ and let I_1, \dots, I_M be disjoint intervals around A_1, \dots, A_M , respectively. Definition (2.4) implies that $\Gamma(\text{Ai}, \cdot)$ is $\mathcal{O}(\sqrt{\gamma})$ close to Ai over $[-X, 0]$ in the norm introduced in (5.10). Thus, for all $0 < \gamma < \gamma_0$ and γ_0 small enough, $\Gamma(\text{Ai}, \bar{\chi})$ has M distinct roots $A'_{1,\sigma} \in I_1, \dots, A'_{M,\sigma} \in I_M$ in $[-X, 0]$. That these are ordered as $A'_{M,\sigma} < \dots < A'_{1,\sigma}$ follows from $A_{M,\sigma} < \dots < A_{1,\sigma}$ and the fact that I_1, \dots, I_M were chosen to be disjoint. The bounds on $A'_{1,\sigma}, \dots, A'_{M,\sigma}$ may be derived by writing $A'_{n,\sigma} = \sum_{\ell \geq 0} \varepsilon^{\ell/6} a_{n,\sigma}^{(\ell)}$, substituting into the equation $\Gamma(\text{Ai}, \bar{\chi}) = 0$, and expanding asymptotically.

The existence of $B_{0,\sigma} > 0$ and the bound on it may be established using Lemma A.1 (with $p = 1 + \bar{\psi}$ and $q = 0$). \square

Appendix B. Proof of Lemma 5.2. Using definition (5.8), we calculate

$$(B.1) \quad \mathcal{A}(\bar{\chi}) - \Gamma(\text{Ai}, \bar{\chi}) = -\frac{\Gamma(\text{Ai}, \gamma^{-1} + \bar{\chi})}{\Gamma(\text{Bi}, \gamma^{-1} + \bar{\chi})} \Gamma(\text{Bi}, \bar{\chi}).$$

To estimate the fraction on the right-hand side, we apply standard theory for Airy functions [2]; see Appendix A. Using Lemma A.1 (with $p = 1$ and $q = \bar{\chi}$), we find that

$$\sup_{\bar{\chi} \in [X, 0]} \left| \exp \left(\frac{4}{3\gamma^{3/2}} + \frac{2\bar{\chi}}{\gamma^{1/2}} \right) \frac{\Gamma(\text{Ai}, \gamma^{-1} + \bar{\chi})}{\Gamma(\text{Bi}, \gamma^{-1} + \bar{\chi})} - \frac{1}{2} \frac{\beta + 1}{\beta - 1} \right| < c_1 \sqrt{\gamma},$$

for some $c_1 > 0$ and γ small enough. Therefore,

$$(B.2) \quad \sup_{\bar{\chi} \in [X, 0]} \left| \frac{\Gamma(\text{Ai}, \gamma^{-1} + \bar{\chi})}{\Gamma(\text{Bi}, \gamma^{-1} + \bar{\chi})} \right| < c_2 \exp \left(-\frac{4 + 6\gamma X}{3\gamma^{3/2}} \right),$$

for some $c_2 > 0$. Next, $\sup_{\bar{\chi} \in [X, 0]} |\Gamma(\text{Bi}, \cdot)| \leq c_3$ for some $c_3 > 0$, since Bi and Bi' are uniformly bounded over $[X, 0]$. Combining these estimates, we find

$$(B.3) \quad \sup_{\bar{\chi} \in [X, 0]} |\mathcal{A}(\bar{\chi}) - \Gamma(\text{Ai}, \bar{\chi})| < c_4 \exp \left(-\frac{4 + 6\gamma X}{3\gamma^{3/2}} \right),$$

for some $c_4 > 0$ and for all γ small enough.

Next, differentiating (B.1), we calculate

$$(B.4) \quad \begin{aligned} \mathcal{A}'(\bar{\chi}) - \Gamma(\text{Ai}', \bar{\chi}) &= \left(\frac{\Gamma(\text{Ai}, \gamma^{-1} + \bar{\chi}) \Gamma(\text{Bi}', \gamma^{-1} + \bar{\chi})}{[\Gamma(\text{Bi}, \gamma^{-1} + \bar{\chi})]^2} - \frac{\Gamma(\text{Ai}', \gamma^{-1} + \bar{\chi})}{\Gamma(\text{Bi}, \gamma^{-1} + \bar{\chi})} \right) \Gamma(\text{Bi}, \bar{\chi}) \\ &\quad - \frac{\Gamma(\text{Ai}, \gamma^{-1} + \bar{\chi})}{\Gamma(\text{Bi}, \gamma^{-1} + \bar{\chi})} \Gamma(\text{Bi}', \bar{\chi}). \end{aligned}$$

Using Lemma A.1, we may bound the term in parentheses by

$$\frac{c'_1}{\sqrt{\gamma}} \exp\left(-\frac{4+6\gamma X}{3\gamma^{3/2}}\right),$$

for some $c'_1 > 0$. Next, $\Gamma(\text{Bi}, \bar{\chi})$ was uniformly bounded by a constant c_3 above. Also, the term $\Gamma(\text{Bi}', \bar{\chi})$ may be bounded by a constant c'_3 , since

$$\Gamma(\text{Bi}', \bar{\chi}) = \text{Bi}'(\bar{\chi}) - \sqrt{\gamma} \beta \text{Bi}''(\bar{\chi}) = \text{Bi}'(\bar{\chi}) - \sqrt{\gamma} \beta \bar{\chi} \text{Bi}(\bar{\chi}),$$

and the term multiplying it in (B.4) was bound in (B.2). These inequalities yield, then,

$$(B.5) \quad \|\mathcal{A}'(\cdot) - \text{Ai}'(\cdot)\|_{[X,0]} < c'_2 \gamma^{-1/2} \exp\left(-\frac{4+6X\gamma}{3\gamma^{3/2}}\right),$$

for some $c'_2 > 0$ and for all γ small enough. Equation (5.11) follows now from (B.3) and (B.5). \square

Appendix C. Proof of Lemma 5.3. Definition (5.9) yields

$$(C.1) \quad \mathcal{B}(\gamma^{-1}\bar{\psi}) - \Gamma(\text{Bi}, \gamma^{-1}(1+\bar{\psi})) = -\frac{\Gamma(\text{Bi}, \gamma^{-1}\bar{\psi})}{\Gamma(\text{Ai}, \gamma^{-1}\bar{\psi})} \Gamma(\text{Ai}, \gamma^{-1}(1+\bar{\psi})).$$

To estimate the right-hand side, we work as in Appendix B. Using Lemma A.1 twice (once with $p = \bar{\psi}$, $q = 0$ and once with $p = 1 + \bar{\psi}$, $q = 0$), we obtain

$$(C.2) \quad \sup_{\bar{\psi} \in [\Psi_R, \Psi_L]} \left| E(\gamma^{-1}(1+\bar{\psi})) \frac{\Gamma(\text{Bi}, \gamma^{-1}\bar{\psi})}{\Gamma(\text{Ai}, \gamma^{-1}\bar{\psi})} \Gamma(\text{Ai}, \gamma^{-1}(1+\bar{\psi})) \right| \\ < c_1 \gamma^{1/4} \left[\frac{E(\gamma^{-1}(1+\Psi_L))}{E(\gamma^{-1}\Psi_L)} \right]^2,$$

for some $c_1 > 0$ and γ small enough.

Next, differentiating (C.1), we calculate

$$\mathcal{B}'(\gamma^{-1}\bar{\psi}) - \Gamma'(\text{Bi}, \gamma^{-1}(1+\bar{\psi})) = -\frac{\Gamma(\text{Bi}, \gamma^{-1}\bar{\psi})}{\Gamma(\text{Ai}, \gamma^{-1}\bar{\psi})} \Gamma(\text{Ai}', \gamma^{-1}(1+\bar{\psi})) \\ + \left(\frac{\Gamma(\text{Bi}, \gamma^{-1}\bar{\psi}) \Gamma(\text{Ai}', \gamma^{-1}\bar{\psi})}{[\Gamma(\text{Ai}, \gamma^{-1}\bar{\psi})]^2} - \frac{\Gamma(\text{Bi}', \gamma^{-1}\bar{\psi})}{\Gamma(\text{Ai}, \gamma^{-1}\bar{\psi})} \right) \Gamma(\text{Ai}, \gamma^{-1}(1+\bar{\psi})).$$

Using Lemma A.1 and Corollary A.1 to estimate the right-hand side, we find

$$(C.3) \quad \sup_{\bar{\psi} \in [\Psi_R, \Psi_L]} |E(\gamma^{-1}(1+\bar{\psi})) [\mathcal{B}'(\gamma^{-1}\bar{\psi}) - \Gamma'(\text{Bi}, \gamma^{-1}(1+\bar{\psi}))]| \\ < c'_1 \gamma^{-1/4} \left[\frac{E(\gamma^{-1}(1+\Psi_L))}{E(\gamma^{-1}\Psi_L)} \right]^2,$$

for some $c'_1 > 0$ and γ small enough.

The desired result follows from (C.2) and (C.3). \square

REFERENCES

- [1] M. ABRAMOWITZ AND I. A. STEGUN, *Handbook of Mathematical Functions*, Dover, New York, 1965.
- [2] C. M. BENDER AND S. A. ORSZAG, *Advanced Mathematical Methods for Scientists and Engineers*, Appl. Math. Sci. 35, Springer-Verlag, New York, 1999.

- [3] P. N. BROWN, G. D. BYRNE, AND A. C. HINDMARSH, *VODE: A variable-coefficient ODE solver*, SIAM J. Sci. Statist. Comput., 10 (1989), pp. 1038–1051.
- [4] E. A. CODDINGTON AND N. LEVINSON, *Theory of Ordinary Differential Equations*, McGraw-Hill, New York, 1955.
- [5] U. EBERT, M. ARRAYÁS, N. TEMME, B. P. SOMMEIJER, AND J. HUISMAN, *Critical conditions for phytoplankton blooms*, Bull. Math. Biol., 63 (2001), pp. 1095–1124.
- [6] P. G. FALKOWSKI, R. T. BARBER, AND V. SMETACEK, *Biogeochemical controls and feedbacks on ocean primary production*, Science, 281 (1998), pp. 200–206.
- [7] K. FENNEL AND E. BOSS, *Subsurface maxima of phytoplankton and chlorophyll: Steady-state solutions from a simple model*, Limnol. Oceanogr., 48 (2003), pp. 1521–1534.
- [8] S. GHOSAL AND S. MANDRE, *A simple model illustrating the role of turbulence on phytoplankton blooms*, J. Math. Biol., 46 (2003), pp. 333–346.
- [9] M. H. HOLMES, *Introduction to Perturbation Methods*, Texts Appl. Math. 20, Springer-Verlag, New York, 1995.
- [10] J. HUISMAN, P. VAN OOSTVEEN, AND F. J. WEISSING, *Critical depth and critical turbulence: Two different mechanisms for the development of phytoplankton blooms*, Limnol. Oceanogr., 44 (1999), pp. 1781–1787.
- [11] J. HUISMAN, N. N. PHAM THI, D. M. KARL, AND B. P. SOMMEIJER, *Reduced mixing generates oscillations and chaos in the oceanic deep chlorophyll maximum*, Nature, 439 (2006), pp. 322–325.
- [12] J. HUISMAN AND B. P. SOMMEIJER, *Population dynamics of sinking phytoplankton in light-limited environments: Simulation techniques and critical parameters*, J. Sea Res., 48 (2002), pp. 83–96.
- [13] W. HUNDSDOERFER AND J. G. VERWER, *Numerical Solution of Time-Dependent Advection-Diffusion-Reaction Equations*, Ser. Comput. Math. 33, Springer-Verlag, New York, 2003.
- [14] H. ISHII AND I. TAKAGI, *Global stability of stationary solutions to a nonlinear diffusion equation in phytoplankton dynamics*, J. Math. Biol., 16 (1982), pp. 1–24.
- [15] C. A. KLAUSMEIER AND E. LITCHMAN, *Algal games: The vertical distribution of phytoplankton in poorly mixed water columns*, Limnol. Oceanogr., 46 (2001), pp. 1998–2007.
- [16] K. H. MANN AND J. R. N. LAZIER, *Dynamics of Marine Ecosystems*, Blackwell Science, Oxford, UK, 1996.
- [17] N. N. PHAM THI, J. HUISMAN, AND B. P. SOMMEIJER, *Simulation of three-dimensional phytoplankton dynamics: Competition in light-limited environments*, J. Comput. Appl. Math., 174 (2005), pp. 57–77.
- [18] I. STAKGOLD, *Boundary Value Problems of Mathematical Physics*, Vol. II, Macmillan, New York, 1968.
- [19] H. E. DE SWART, H. M. SCHUTTELAARS, AND S. A. TALKE, *Initial growth of phytoplankton in turbid estuaries: A simple model*, Continental Shelf Research, (2007), to appear; doi: 10.1016/j.csr.2007.09.006.
- [20] K. YOSHIYAMA AND H. NAKAJIMA, *Catastrophic shifts in vertical distributions of phytoplankton. The existence of a bifurcation set*, J. Math. Biol., 52 (2006), pp. 235–276.